DEFORMATION OF SUPERPLASTIC ALLOYS AT RELATIVELY LOW STRESS RATES

TABLE OF CONTENTS

DEFORMATION OF SUPERPLASTIC ALLOYS AT RELATIVELY LOW STRAIN RATES

Dionysios Grivas

Materials and Molecular Research Division, Lawrence Berkeley Laboratory
and Department of Materials Science and Mineral Engineering,
University of California, Berkeley, California 94720

ABSTRACT

The superplastic and sub-superplastic creep properties of Pb-Sn eutectic and Al-Zn eutectoid alloys were studied. Various thermomechanical treatments we tested to check the possibilities of whether the subsuperplastic deformation mechanism is affected by these treatments. All thermomechanical histories were found to reveal the same stress exponent, which is believed to be indicative of the predominant mechanism. The mechanical data in the low stress region lead us to suggest that dislocation glide is the predominant mechanism in this region. At higher stresses extensive grain boundary sliding takes place and the dislocation movement is directed to relieve the stress concentration developed by the grain movement.

The thermomechanical history of the ingot has a marked effect on the steady state strain rate which cannot be accounted for by the mean grain diameter, indicating that another microstructure characterization parameter is required for the complete representation of the steady state creep data of superplastic alloys. It was found that the creep resistance of the Al-Zn eutectoid alloys can be improved drastically by the additional thermal treatment of homogenizing the alloy in the α region and slow cooling to induce the plate like microstructure. The thermomechanical history was also found to have an effect on the total elongation before failure in this alloy.

GENERAL

In 1934, Pearson (1) reported a 2000% extension in a hot extrusion test on Bi-Sn eutectic wire. Earlier, Rosenhaim et al. (2) had observed that a copper zinc aluminum tertiary eutectic alloy "behaved differently from ordinary crystalline materials such as aluminum but very similar to pitch glass". Around 1945, this phenomenon was termed "superplasticity" as a direct translation of a Russian term introduced by Bochran and Sriderskian (3) to describe these extraordinary deformations.

Superplasticity did not draw much attention until the early sixties. Interest in this subject was renewed after the publication of Underwood's (4) general review on superplasticity in 1962. In the past 15 years an ever-increasing effort by scientists and engineers has been directed towards understanding this phenomenon which is reflected in a rapidly growing number of scientific papers and technical sessions on this subject. The interest in superplasticity is two-fold: 1) to exploit superplasticity for commerical purposes, and 2) to understand the operating mechanism of this type of deformation.

Superplasticity did not obtain the wide use nor did it lead to any "commercial bonanza" as was expected ten years ago (5). The acceptance and utilization of these materials has been slow but consistent. Now that superplastic metals are commercially available and with the introduction of cheaper and more widely used alloys such as the high carbon steels developed at Stanford University (6), superplasticity seems to be becoming a viable forming technique. Many new forming techniques are being investigated, amongst which are the superplastically deformed diffusion bonded structures (7) developed by Rockwell International, which will open new doors to the utilization of superplastic alloys.

Besides the advantages of superplastic deformation, which include reduced forming pressure, cost savings due to extremely close tolerances, wastage minimization and uniform microstructure of the product, which leads to uniform reproducible mechanical properties, there are also some important disadvantages which weaken the full impetus of superplastic materials. These materials, for instance, exhibit inferior creep properties to those obtained by conventional forming routes, require slow deformation rates and relatively high and closely controlled temperatures, and finally exhibit low strengths due to their fine microstructure. With more of these disadvantages eliminated, these materials will gain more widespread applications.

INTRODUCTION

The Role of the Stress Exponent in Superplasticity

Superplasticity can be defined in very general terms as the mode of deformation that leads to essentially neck free deformation, and consequently to very large deformations before failure. In general superplasticity can be broadly classified into two general groups: one due to repeated phase transformation caused by thermal cycling and the other due to special microstructural conditions. Only the latter type of superplasticity will be considered in this thesis. Two requirements must be fulfilled for a microstructural superplasticity to occur. 1) The deformation temperature must be higher than .5 of the melting temperature and 2) the microstructure of the alloy must be fine and stable. The flow stress is related to the strain rate by the empirical relationship

$$\dot{\epsilon} = k\sigma^n \qquad \text{Equation 1}$$

where $\dot{\epsilon}$ is the strain rate, σ is the applied stress and n is the stress exponent and k is a constant. This stress exponent has been shown to have a direct effect on the amount of ductility (9,10). For best ductility, localized deformation should be avoided, especially necking. The contribution of the stress exponent to stable flow can be demonstrated by the following analytical argument. Equation 1 can be rewritten as $\dot{\epsilon} = k(\frac{L}{A})^n$ where L is the load imposed onto the speciman through area A. The strain rate of an incompressible material at any point along the specimen is given by

$$\dot{\epsilon} = \frac{1}{\epsilon}\frac{d\epsilon}{dt} \quad \text{or since} \quad \frac{d\epsilon}{dt} = -\frac{1}{A}\frac{dA}{dt} \quad \text{equation 1 becomes}$$

$$-\frac{1}{A}\frac{dA}{dt} = k(\frac{L}{A})^n \quad \text{and} \quad \frac{dA}{dt} = -k\,L^n\,A^{(1-n)} \qquad \text{Equation 2}$$

This last equation shows that dA/dt becomes increasingly independent of A as n approaches unity, and when $n = 1$, the stress exponent for a Newtonian viscous fluid, the value of dA/dt is independent of A. It can, therefore, be concluded that the best possible superplastic behavior requires the lowest possible value of n. This point has been supported by various investigations and the stress exponent most readily associated with superplasticity is $n = 2$ (11). In the course of the past 15 years some investigators have argued that n depends on the strain rate reaching a minimum value of around 2, as is shown in Fig. 1 (12), while others have maintained that there is a range of strain rates over which the stress exponent maintains the constant value of approximately 2 (13). Hayden et al. (14) reported that an $n = 2$ region extends over 4 orders of magnitude of strain rates. This implies that it is unlikely that this $n = 2$ region is a transition region between a high n value and a low n value.

The stress exponent has been used in theoretical studies as well to infer the characteristics of the predominant deformation mechanism, as it is believed that the value of the stress exponent is indicative of the predominant mechanism.

Studying Superplasticity

In studying the deformation of materials, relationships between the three parameters strain, strain rate and stress are sought. In Fig. 2, we show the relationship between the variables and the experimental techniques used to study them. In general there are two main approaches to these studies:

1) the phenomenological approach, which does not concern itself with the actual mechanism of deformation, but is satisfied if the mathematical formulation can represent a large number of experimental observations, and

2) the mechanistic or slip approach in which the predominant mechanism is described in an algebraic form. From this formulation, the mechanical properties (flow stress, creep properties, etc.) may be predicted for a wide spectrum of conditions, including variations in the stress, strain rate, temperature, microstructure and history.

Research following the phenomenological approach is being advocated by E. Hart and C.Y. Li (15). Their latest and most controversial theory (16) suggests that all deformation can be described incrementally by the differential equation

$$d \ln \sigma = \gamma \, d \varepsilon + \nu \, d \ln \dot{\varepsilon} \qquad \text{Equation 3}$$

For this equation to be integratable, there must be an integrating factor such that $dy = F d\varepsilon$ where y is called the hardness parameter. Hedworth and Stonewell (17) assumed that the superplastic deformation is viscous, in which case the deformation is independent of the path and substituted $\gamma = 0$ which leads to $(d\ln\sigma/d\ln\dot{\varepsilon}) = n$. This is a simplification of Hart's theory, which stated that $\sigma = \sigma(y,\dot{\varepsilon})$, while Hedworth and Stonewell (17) assumed $\sigma = \sigma(\dot{\varepsilon})$. Hedworth et al. have reported that

through applying the stress relaxation test and the aforementioned analysis, they have obtained a value for n equal to 2.

Dorn (13) and his associates published a review which most representataively exemplifies the mechanistic approach to deformation studies. These authors suggested that the equation

$$\frac{\gamma kT}{DoGb} = A\left(\frac{\tau}{G}\right)^n \left(\frac{b}{d}\right)^m e^{-\Delta H/kT} \qquad \text{Eq. 4}$$

can represent the steady state creep behavior of a number of important systems, including superplastic alloys. The parameters in Equation 4 appear in the Appendix. They specifically suggested that as τ is decreased, a superplastic material will pass through 3 distinct regions of steady state creep. In each one, a particular variant of the above equation will be obeyed.

1) When n is sufficiently large they predict a "conventional" steady state creep, controlled by a dislocation climb mechanism. Hence, they anticipate a stress exoponent in the range 4~7, an apparent activation energy ΔH in the order of that for self diffusion and a creep rate independent of the microstructure ($m = 0$).

2) For smaller τ they suggest a region of well-defined "superplastic creep". On semi-empirical grounds they anticipate $n = 2$ ΔH in the order of that for grain boundary diffusion and an inverse square grain size dependence. The exact characteristics of this mechanism have not yet been fully understood. It is generally believed that the predominant mechanism in these strain rates is grain boundary sliding and grain boundary rotation. This has been supported by experiments in which the surface of a virgin specimen was scratched and then the misalignment of the scratches after deformation was observed (19,20,21,22). Other evidence which support grain boundary movement as the operating

mechanism during superplastic flow are the very little elongation of the grains during deformation (22,30), the progressive removal of crystallographic texture at superplastic strain rates (23,24), and the marked surface relief (18,21,22,25). Opponents of these types of experiments argue that surface observations are not necessarily indicative of what takes place in the bulk. The point, which is not widely agreed upon, is the process of mass accomodation at the triple points, a necessary condition to maintain mass continuity and avoid premature failure. Theories such as grain boundary diffusion (26) or lattice diffusion (9,27,28), grain boundary dislocation movement (58), matrix dislocation movement (21,29), and grain boundary migration (31) have been put forward as the accomodating mechanism. TEM studies, either of deformed specimens or in situ, are conflicting and ambiguous. While some reports suggest the importance of dislocations in this mode of deformation, others disagree. Dislocations have been observed (20,21,29) in a few cases but the interpretation of TEM observations is difficult, since dislocations need to travel a only short distance to be lost at nearby grain boundaries during unloading or cooling to room temperature and subsequent specimen preparation. Experiments have been designed which introduce precipitates to trap the dislocations (30,32), but this is possible only for one of the two phases of the alloy involved. In situ experiments (33,34) have been performed, but since the foil is so thin, it cannot confidently be concluded that the observed mode of deformation corresponds to the superplastic mechanism.

3) At even lower stresses, Bird, Mukherjee, and Dorn predict a behavior dominated by Coble creep (35), which involves atom movement through the grain boundaries with an activation energy of the order of grain boundary diffusion, an inverse cube grain size dependence, and a stress

exponent equal to one.

Bird et al. have fit Avery and Backofen's (27) Pb-Sn eutectic and Ball and Hurchinson's (21) creep data on Zn-22Al eutectoid to different variants of equation (1). They argue that both alloys show clear regions of conventional and superplastic creep. They also found evidence for Coble creep in the Zn-22Al, but were unable to establish its existence for the Pb-Sn eutectic alloy due to the unavailability of suitable data. Vaidya, Murty and Dorn (36) and latter Misro and Mukherjee (37) have reinvestigated the steady state creep of Zn-22Al. Both sets of investigators claim verification of the Bird, Mukherjee, and Dorn representation. Work performed by D. Grivas (38) on Pb-Sn eutectic showed that, for stresses corresonding to the climb and to the superplastic region, the data are satisfactorily represented by the above model, but for stresses corresponding to the sub-superplastic region the stress exponent was found to be equal to three. This observation was verified later by Mohammed and Langdon (39) for the Pb-Sn eutectic alloy. Such a behavior would agree with most of the data availabie which indicates a decrease and then an increase in the value of n as the stress is progressively increased, as mentioned earlier (Fig. 1).

Either one of the following two techniques were used to obtain the stress exponent: either a load change test during a creep test or a strain rate change test during a tensile test.

In the load change test, the specimen is left to creep until steady state is reached and then the load is changed and the new steady state is observed. The stress exponent is then evaluated as

$$n = \frac{\ln \dot{\varepsilon}_2/\dot{\varepsilon}_1}{\log \sigma_2/\sigma_1} \qquad \text{Equation 5}$$

Fig. 3 shows the schematic representation of a typical strain rate change test on a tensile specimen. The specimen is pulled at a crosshead speed V_1 until the load passes a maximum. Just after the load has reached its maximum, the crosshead speed is suddenly changed to V_2 ($V_1 < V_2$). When passing the maximum load under this higher speed, the crosshead speed is suddenly lowered to the value of V_3. This procedure continues over a wide range of crosshead speeds and again a similar equation is used

$$n = \frac{\log V_2/V_1}{\log (P_2/P_1)} \qquad \text{Equation 6}$$

There are variations to these techniques as far as the value of the P's are concerned. These are shown in Fig. 3, where the P's may be chosen to

(1) correspond to flow stresses just after yielding (17)

(2) correspond to the maximum flow stresses (40,41,42)

(3) correspond to flow stresses after a constant amount of strain (9),

$$n = \frac{\ln V_2/V_1}{\ln P_A/P_{A'}} \qquad \text{Equation 7}$$

(4) correspond to the flow stresses immediately before and after the crosshead speed change (17).

$$n = \frac{\log V_2/V_1}{\log P_B/P_{B'}} \qquad \text{Equation 8}$$

The greater bulk of the data mentioned above have been obtained on tensile type specimens.

It is clear from the above discussion that the stress exponent relates the strain rate to some stress. It does not follow though that all the n values obtained by the different variants of the technique should be equal, a point which has many times been assumed to be true. There are some assumptions involved, which need to be borne

in mind when an analysis of these experimental data is being made. We will return to this point later in the main text of this thesis.

Correlation Between Microstructure and Superplasticity

As mentioned earlier, one of the requirements for superplasticity to take place is a fine microstructure. It is this requirement which has led the investigators to use alloys of eutectic or eutectoid or near eutectic-eutectoid composition. A fine structure in the eutectic alloys is obtained by a series of mechanical workings of the cast and subsequent recrystallization. The most widely studied superplastic alloy of eutectic composition is the Pb-Sn alloys. Tiller and MrDjenovich (43) have shown that the microstructure of the cast Pb-Sn eutectic can vary as a function of the cooling rate. Slow cooling rates result in large interconnected phases, while rapidly cooled specimens have more globular structures. Turnball and Treaftis (44) reported that cold work accelerates the formation of Sn precipitates in the lead rich phase, which nucleate in the matrix, while for specimens with no cold work the precipitates tend to nucleate in the vicinity of the grain boundary. Besides the cold work and recrystallization procedure, alloys of eutectoid composition can show superplasticity by fast quenching the specimen from the homogeneous phase to obtain a fine two phase structure. Packer et al. (45) compared the deformation characteristics of the two preparation techniques on an Al-Zn eutectoid alloy and attributed their differences to the texture introduced during the mechanical working. The total elongation of superplastic alloys was shown by Morrison (41) to depend on the amount of mechanical working prior to their deformation while Mohamed et al. (11) showed that the total ductility is influenced greatly by the mean grain size of the

alloy. Holt and Backofen (46) reported that Al-Cu eutectic alloys of different thermomechanical history but of similar mean grain diameter behave differently. While the mechanically worked and annealed specimens exhibited superplastic elongations, the specimens, which were only annealed did not reveal any considerable deformation before failure. They attributed this difference to the grain boundary characteristics resulting from the different histories. They argued that annealing the cast structure results in irregular interface boundaries which could not accomodate the imposed strain. Avery and Backofen (27) observed similar results with the Pb-Sn eutectic alloy. They reported that the stress exponent of the as cast specimen was high for all strain rates and tensile failure involved necking plus extensive formation of internal voids, all characteristic of non-superplastic deformation. On the other hand extruded and recrystallized specimens tested under similar conditions exhibited superplasticity. They attributed this difference in deformation behavior to the morphology of the grain structure resulting from the extra mechanical treatment performed on the cast ingot. The flow stress of the as cast structure was found to be much higher than that of the worked and recrystallized structure at all strain rates. It appears that superplasticity is highly dependent on the thermomoechanical history of the specimen.

Aim of Thesis

In the previous chapters the relationship between the stress exponent and the superplastic behavior was reviewed. The techniques used to obtain the stress exponent were discussed and their incompatibility was mentioned. The controversy as far as the mechanism operating at stresses below the superplastic region and how this is reflected in the difference of the value of the stress exponent was pointed out. Finally we discussed

how superplasticity can be obtained by a variety of thermomechanical treatments which have varied effects on the superplastic behavior.

This present research project was undertaken in order to:

1. Study the superplastic and subsuperplastic deformation characteristics of two phase systems in the hope of resolving the controversy regarding the operating mechanism at the low stress region, which is reflected on the stress exponent and
2. Study the effect of the thermomechanical history on the mechanical properties of superplastic alloys.

The first objective may appear to be motivated by purely academic interest as deformation at such low strain rates is of no commercial importance. However, it is expected that an understanding of the predominant mechanism at the low stress region might assist in understanding the characteristics of superplastic deformation as these two mechnisms might be operating in a closely related fashion. Consequently understanding the mechanism of superplastic deformation would put us in a position to exploit this very interesting phenomenon to its fullest capacity. An understanding of the effect of the thermomechanical history on superplasticity might yield the best superplastic characteristics which include the fastest deformation rate at the lowest temperature and/or lowest stress (which would result in savings in production expenditure due to the reduction of energy consumption), highest ductility and subsequent creep resistance in operation.

EXPERIMENTAL PROCEDURE

Three ingots of 62 Sn-38 Pb compositions were made by melting 99.999 purity lead and 99.999 purity tin in a graphite cricible. The ingots were then cast in three separate copper molds of 2 1/2 inches, 1 1/2 inches and 1 inch in diameter. The ingots were made from three different heats, but no variation in the purity level is expected, as same the same starting materials were used in each case.

The ingots were given the treatments shown in Table 1. Double shear specimens were made from these rods (Fig. 2). The advantage of the double shear specimens over the tensile specimen is the elimination of the necking problem inherent in tensile specimens until after a substantial strain has occurred. The double shear configuration leads to true constant strain rate conditions thereby permitting a direct comparison between creep and constant strain rate conditions during deformation. Prior to testing, the specimens were kept in dry ice to prevent grain growth. The specimens were annealed at 170° C.

Four specimens of Al-Zn eutectoid composition were supplied by Dr. Fergalli Mohammed of the University of Southern California. The remainder of the specimens were made in the following fashion: 99.999 purity aluminum and zinc were melted in a graphite crucible to obtain a composition of Al-22Zn. The melt was cast in a copper mold 1 1/2 inches in diameter. The ingot was subsequently heated to 350° C for one hour in a stainless steel envelope filled with argon gas and then rolled to 7/8 inch rods. The ingot was heated to 350° C between each pass. It was impossible to work the cast structure at room temperature due to its brittleness at this temperature.

Part of this rod was made into double shear specimens and part

was rolled into plastes 1/8 inch thick. The ingot was heated to 260°C between every two passes. From the plate, tensile specimens were made of the dimensions shown in Fig. 4. The aluminum-zinc specimens were heated at 260°C before testing to obtain the desired microstructures. Creep tests were performed on a creep testing machine, built in the laboratory, as shown in Fig. 5. The strains in the creep test were measured by an LVDT directly attached to the specimen. Because the creep machine was not able to record fast strain rates, fast tests were performed on an Instron machine. Tensile tests were performed on the Instron machine as shown in Fig. 6.

The tests were performed in a silicon oil bath, whose temperature was controlled constant to ±1° C. The mean phase diameter was calculated from optical and electron scanning micrographs by the mean intercept method (52). The mean lead rich phase diameter was computed from the same photographs by drawing at least four lines on every photograph and measuring the individual lengths of each of the lead phases through which the random line had intercepted. The values were averaged for at least 6 photographs, representing different areas of the specimen. Around 300 individual measurements were made for the computation of the mean lead rich phase.

RESULTS

A. The Validity of the Assumptions Made in Computing the Stress Exponent

When computing the stress exponent from the strain rate change test there are some asuumptions made which should be noted and tested for their validity. These assumptions are:

1) That there are no microstructural changes during deformation which could affect the subsequent deformation at another load or strain rate. It has been shown in the literature that the initial texture of a superplastic alloy tends to disappear during superplastic flow (23,24). It has also been stated many times that there is considerable grain growth at the high deformation temperature required for superplasticity. T.H. Alden and H.W. Schadter (22) measured the mean phase diameter of the Al-Zn eutectoid alloy as a function of the amount of straining at constant temperature and strain rate, and reported that the mean phase diameter increased with straining, but examination of the longitudinal and of the transverse section showed no evidence of grain elongation. Similar results were obtained on the Al-Cu eutectic alloy (47) and on the Pb-Sn eutectic alloy (12). This grain growth could be attributed either to the non-equilibrium state of the microstructure or to the deformation or to both.

In an attempt to eliminate possible grain growth due to the non-equilibrium state of the microstructure we annealed the lead tin eutectic alloy for seventy-five days at 170°C to obtain a mean phase diameter of 17.5 μm. This specimen was tested in a creep machine and the data is shown in Fig. 7. The specimen was allowed to creep at each load till the steady state strain rate was clearly observed. The load was then reduced. The duration of the test was approximately twenty-one

hours and no appreciable grain growth due to the phase instability should be expected. In Table II we show the microstructural changes in the longitudinal and cross sections of the crept specimen. The mean phase diameter has changed drastically in both views. In the cross section it has been increased by 4.5 μm, while in the longitudinal it has been increased by 2.3 μm. It can be assumed that the microstructural changes, due to the applied load, tend to make the phase structure more equiaxed. In this mode of deformation, where the deformation direction is perpendicular to the texture introduced by the mechanical work during preparation, the elongated lead rich phase tends to become more globular. When reapplying the load of 198 psi the steady state strain rate obtained is lower than the strain rate expected if no microstructural changes had occurred during previous testing.

2) A second assumption is that there is no work hardening associated with superplastic deformation. The absence of such work hardening should result in the absence of any primary creep during a creep test. This point was supported by Misro & Mukherjee (37) and by Vadiya Murty and Dorn (36) for the Al-Zn eutectoid alloy. Misro and Mukherjee (37) deduced from this observation that "the significant substructural detail pertinent to the rate controlling mechanism was substantially constant from the beginning". On the other hand, stress strain curves presented in the literature (49,21) for Al-Zn eutectoid and for testing conditions corresponding to the superplastic mode of deformation report an appreciable amount of strain hardening which extended over 5% strain. Fig. 8 shows the creep curve of a lead tin eutectic alloy deformed under conditions which had previously been tested to correspond to superplastic deformation. Some primary creep can be seen. This primary creep could be accounted for by the anelastic strain, that is, the time dependent recoverable

strain. To test this point the following experiment was performed: after the steady state was reached, the load was taken off and the recoverable strains measured as a function of time. It was then assumed that the mechanism for the creep was independent of that of the anelastic strain. So the summation of the strain contributions of these two mechanisms should give the actual creep curve. All this is shown in Fig. 8. It can be seen that the anelastic strain does not account for all the primary creep. From this figure and similar figures obtained in the course of this investigation, primary creep was distinctly seen. The portion of it which is due to anealastic strain is not clear from this limited amount of data. In creep tests, depending on whether the load was added or taken off, work hardening or work softening occurred as is shown in Fig. 9. This observation supports the conclusion that there is a certain amount of microstructural change occurring during the first few percent of superplastic creep, until steady state is reached. Similar observations were made on Al-Zn eutectoid specimens.

Due to this work hardening, the value of the stress exponent is not expected to be constant for the strains corresponding to the primary creep. A much better consistency will be observed if the flow stress is related to a strain rate that is independent of the amount of strain. In the case of the creep test, this is the steady state creep rate.

The advantage of the stress relaxation technique is that for a a very small amount of strain on the specimen, it reveals the stress strain rate relationship over a large range of strain rates. In addition, the duration of the test is relatively short so that the problem of grain growth is kept to the minimum. The stress relaxation test is performed on a stiff machine, capable of deforming the material at a constant velocity. Between the load cell and the specimen a stiff spring is

placed. The specimen is deformed to a certain strain and then the machine stopped. The elastic strain on the spring forces the specimen to deform, until equilibrium of the forces is reached. In this mode of deformation

$$\frac{d\tau}{dt} = - G \dot{\gamma}$$

where G is the effective modulus of the specimen and the machine. It has been proposed (17) that a logarithmic plot of $\frac{d\tau}{dt}$ vs τ should reveal the stress exponent value. Stress relaxation experiments performed on the Pb-Sn eutectic alloy revealed two regions of different n values (Fig. 10). At high stress an exponent in the neighborhood of 6.5 was seen while at low stresses the stress exponent took the value 3. The $n = 2$ region which is characteristic of superplasticity was not observed in this mode of testing. Similar results were obtained on Pb-Sn in eutectic at Cornell University (53). It is not clear at this point why Hedworth et al. (17) observed an $n = 2$ region. From our results it seems that the stress exponent which reflects the predominant mechanism at that strain rate region is dependent on the loading manner. In the stress relaxation test, loading is done in an incremental fashion while in the stress or strain rate change test the changes are in discrete units.

B. The Value of the Stress Exponent at Low Stresses

It was mentioned in the Introduction that in a plot of the logarithmic stress versus the logarithmic steady state strain rate at relatively low stressees, the data were divided into two distinct regions of constant slope. Such a plot is shown in Fig. 11 for an aluminum zinc alloy. In this figure, the transition from the superplastic $n = 2$ to the $n = 3$ region can be seen. The numbers in this figure indicate

the order by which the load was applied. Although the tests at the low stresses were of long duration, the data points lay on the same line. In particular, the test on the far left lasted approximately 50 hours for points #1 to #3, during which time grain growth should have occurred, but when the forth load was applied the point lay on the same line. This suggests that the strain rate does not shift due to microstructural changes, as long as the testing is kept in the $n = 3$ region. Consistent with previous reports, a specimen of larger mean phase diameter (2.3μm.) revealed lower strain rates, but the stress exponent was found again in the close neighborhood of 3. In accord with the results obtained from the 1.1 um specimen the strain rate was found not to shift due to microstructural changes that might have occurred during previous straining. The initial mean phase diameter is compared to the mean phase diameter before and after testing in Table III. An increase in the mean phase diameter can be noticed.

Due to the limitations of our creep apparatus, it was not possible to apply loads corresponding to the superplastic region and return to the $n = 3$ region in the aluminum-zinc alloy. A similar type of experiment was performed onthe lead-tin eutectic alloy. The sequence by which the load was applied is shown by the direction of the arrow (Fig. 12). Reducing the loads from the superplastic region revealed the $n = 3$ region. Applying now a set of loads corresponding to the superplastic regions shifts the curve to a lower strain rate value appropriate for the new grain size, upon application of loads in the $n = 3$ region, the curve seems to have shifted for that region also. This, too, points out the importance of the microstructural changes during deformation. The numbered points on the left indicate the results of a stress cycling experiment performed on a lead tin eutectic

alloy, similar to those performed on the aluminum zinc. The results are consistent with Fig. 11. The strain rate is only dependent upon the initial microstructure in the $n = 3$ region. The data from Specimen 2 are a bit higher than those of Specimen 1, most likely due to the microstructural changes that occurred during testing in the superplastic region.

The creep curves of specimens deformed under stresses corresponding to the $n = 3$ region revealed considerably longer primary strains than if deformed under the superplastic mode. Fig. 13 shows a typical creep curve for the lead tin eutectic alloy. In this figure the anelastic strain is shown and by no means could it account for the primary creep. We obtained similar results for the aluminum zinc alloy, that is, extensive primary creep for loads in the $n = 3$ region (Fig. 14). Work hardening and work softening were observed for this region, too.

It has been proposed that a diffusional process is dominating the deformation rate in the low stress region. This point was supported by the stress exponent equal to one (36,37) in the Al-Zn eutectoid alloy. The above tests on Al-Zn revealed a stress exponent equal to 3 for this alloy. To test the possibility that the predominant mechanism, which is reflected in the stress exponent, depends on the thermomechanical history of the specimen, an alternative specimen preparation procedure was followed. One of the specimens which had exhibited an $n = 3$ region was homogenized in the α region for 24 hours and then ice quenched to reveal a fine two-phase microstructure. The specimen was consequently annealed for 15 minutes at 250°C and then tested. The results are shown in Fig. 15. Again, the stress exponent found is very close to the value 3. This experimental evidence argues against a diffusional mechanism as being the predominant deformation mechanism at these low stresses.

If, however, the predominating mechanism at these stress levels is a diffusional one, no primary creep is expected. Misled by this assumption, the experimentalist might not wait long enough for steady state to be obtained at these low stress levels. In Fig. 16, we show a plot of log τ versus log $\dot{\gamma}$ for zinc aluminum alloy which was left to crrep about 5% the every load was changed. At low stresses, a region with a stress exponent in the neighborhood of 1 is seen. This stress exponent can be attributed to a diffusional process consistent with the assumption made in the beginning of the paragraph.

C. A Study of the Phase Growth Behavior of the Lead Tin Eutectic Alloy

In Fig. 17 we show a logarithmic plot of the mean phase diameter vs the annealing time at a constant temperature for the 3 specimens investigated. In the same plot we include the data reported by Avery and Backofen (27) and Zehr and Backofen (12). The data points reveal parallel straight lines of slope 1/7.15. An Arrhenius plot of the mean phase diamter versus the inverse annealing temperature used for the computation of the activation energy for phase growth is shown in Fig. 18.

The test was conducted in the following manner: The mechanically worked igot was sliced into sections of 1/8 of an inch thickness and stored in dry ice. Each section was allowed to reach room temperature and then placed in a preheated oil bath for 23 hours. The specimen was then stored again, in dry ice (for not more than 3 days) until the specimen was prepared for metallographic observation. Owing to the small dimensions of the specimen, the time to reach the annealing temperature can be assumed to be very short. Furthermore, as discussed earlier, the grain growth rate is relatively small and therefore, the total amount of grain growth, until the specimen reaches the environment

temperature, can be considered negligible. In studies of the grain growth of pure metals, where the rate of growth is very fast, this point has to be taken into consideration. The data of the Arrhenius plot reveal a slight curvature; the best fit straight line through these points gives an activation energy equal to 4.10 kcal/mole. This curvature indicates that there is another parameter involved in the activation energy for phase growth other than the temperature dependence. The variation of the solubility of the one element into another at different temperatures could have some effect on the phase growth characteristics of the Pb-Sn eutectic alloy. It is interesting to note that a similar type of curvature in an Arrhenius plot for the computation of the activation energy for superplastic deformation was observed by D. Grivas (51) on the eutectic Pb-Sn and on the eutectoid Al-Zn by Ball and Hutchinson (21).

D. The Dependence of Some of the Mechanical Properties of Superplastic Alloys on the Thermomechanical History of the Specimen

a) Studies on the lead tin eutectic alloy.

In Fig. 19, the mean phase diameter is plotted against the mean lead rich phase. The data points fall in two distinct families of lines. It is interesting to note that for the same value of the mean phase diameter, two different values of the lead rich mean phase diameter were obtained. A series of experiments were then conducted to study the influence of the variation of the mean lead rich phase on the creep properties of these alloys. Specimens of 2A history were annealed for times necessary to give 1) a mean phase diameter similar to the 1A specimen and 2) a mean lead rich diameter similar to the 1A specimen. The results are shown in Fig. 20. The data points lie

on three different lines. Two distinct regions of constant slope can be seen for each test. At higher stresses, the stress exponent takes the value 2, characteristic of superplastic deformation, while at lower stresses the n value takes the value 3. It can be seen that the data from the 2A specimens are close, and the specimen with the higher mean phase diameter gives the lower strain rate. Specimen 1A revealed a much faster steady state strain rate than the 2A specimen, even though the temperature and mean phase diameter were held constant. At this point, the difference in the creep properties was attributed to the difference in the thermomechanical history of each specimen. Another variation in the thermomechanical history was tested by specimen 3A. The data obtained were represented in the form proposed by Bird, Murkerjee and Dorn, which has been shown to satisfactorily represent the superplastic steady state creep properties of lead tin eutectic alloys (51). The mean phase diameter exponent m was taken as 2 and the activation energy for deformation equal to 11.5 kcal/mole. These values are well accepted for the superplastic mode of deformation of this alloy (51). Fig. 21 shows the logarithmic plot of the $\frac{\nu kT}{DoGb}\left(\frac{b}{d}\right)^2 e^{-\Delta H/kT}$ versus τ/G. Three lines of constant $n = 2$ slope are drawn through the data points. In this Figure, the open and closed symbols indicate the results from specimens of the same ingot but with different mean phase diameters, as shown in the figure caption. The data from the different mean phase diameters of specimens 1A and 2A coalesced into two lines. This indicates the validity of the above equation as far as the microstructure characterization parameter d^{-m} is concerned, for each set of specimens with the same history. For specimens of different history, the microstructure characterization parameter d^{-m} cannot

make the appropriate adjustments required for the data to scale to a general curve. This is a point which is not taken into account by Bird, Murkherjee and Dorn's formulation nor is mentioned by the authors who propose mechanisms for superplastic deformation. The three parallel lines give different values of the constant A . These values are shown in Table IV. In Fig. 22 we show the results obtained from specimens 1A, 1B, 1C and 2A, 2B: that is, the specimens that had similar cooling rates as they were machined from the same ingot but had undergone a variety of mechanical working before being made into specimens. The data of each ingot are quite similar. It appears that for a certain cooling rate history the variation in the amount of mechanical working has no effect.

In photo 1 we show the typical microstructure of specimens 1A and 2A after 120 hours of annealing at 170°C. The black area is the lead rich phase while the white area is the tin rich phase. The lead rich phase seems to be rather globular with a large amount of connectivity between these phases. From the phase diagram we see that the solubility of lead in tin is very little at all temperatures, while the solubility of the tin in lead varies from 19% weight at the eutectic temperature to a few percent at room temperature. It is expected, therefore, that annealing the specimen at a temperature below the eutectic temperature, the excess tin in the lead phase will precipitate out. Such precipitates are shown in Photographs 1 and 2. To ensure that indeed these bright areas were tin precipitates, a specimen was examined under the scanning microscope. In photo 3 we show the X-ray analysis performed on the various regions. The letters below the X-ray pictures correspond to the areas on the photograph bearing the same letter. As it can be seen from the analysis, the areas a and b seem to be the

same, consisting mostly of pure tin, while area d seems to consist of mostly lead; however, the particle c gives peaks of both tin and lead. We believe that the lead peak appeared in this case because the X-rays came from an area larger than the particle which includes lead as well. The minimum area from which a reliable X-ray analysis can be performed in this scanning microscope is 1 μm. There is no doubt that the precipitates in these photographs are tin precipitates. The tin phase is divided into many grains as shown in photo 4. Because of the difference in the hardness and etching characteristics of the two phases, the grains of the lead rich phase were not revealed. The lead and the tin grains making up the two phases can be seen in SEM photographs of the deformed Pb-Sn eutectic alloy reported by Hazzledine and Newbury (25). Photo 5 shows the microstructure of an as-cast specimen. The microstructure is quite fine and globular. The major difference between the as-cast microstructure and the worked and recrystallized one lies in the amount of tin precipitation in the lead rich phase. While the as-cast structure revealed no precipitation, the recrystallized one exhibited extensive precipitation. It seems that the dislocations introduced during the mechanical working behave as sites for the heterogeneous nucleation of the tin precipitates. Turnball and Treaftis (44) have shown that cold working a lead alloy supersaturated with tin accelerates the rate of the tin precipitation. The same authors have reported that the precipitation in the cold worked specimen occurred in the grain matrix while precipitation in the as-cast alloy occurred in the neighborhood of the grain boundary. All of the two phase alloys reported by Johnson (10) to exhibit superplasticity show a high solubility of one element into another at the eutectic or eutectoid temperature. This solubility decreases rapidly with decreasing temperature. The variation in the solubility limit with temperature of these

alloys occurs in one of the two phases. Similarly with the Pb-Sn alloy studied here, precipitates in one of the two phases can be seen in a number of microstructures shown in the literature which exhibit superplasticity, such as the Al-Mg (20), Al-Zn (30,32), Fe-C (6). On the other hand the Al-Ni, Al-Fe, Al-Sn (46) eutectic systems which have been reported not to be superplastic do not show any solubility even at high temperatures. In fact the eutectic Al-Ni and Al-Fe are composed of two intermetallic phases. It was mentioned in the introduction that the as-cast structure which does not exhibit precipitates does not show any superplasticity either. From all the above observations it seems that superplasticity is closely related to a precipitation reaction. Whether this precipitation has an effect on the microstructure stability or whether it directly influences the superplastic mechanism is to be seen with further experimentation.

b) Studies on the aluminum zinc eutectoid alloy.

The effect of the thermomechanical history on the steady state creep properties of the Al-Zn eutectoid were studied in the following experiments: Specimens of two different histories were tested. One set of specimens underwent an extra treatment of being homogenized at 350°C for 20 hours and then quenched in ice to reveal the fine microstructure shown in photo 6a. In photo 6b the residual grain boundary of the α (Al) phase can be seen, indicating that the transformation from $\alpha + \beta$ to α had occurred, and that the α grains had grown very large. In the next photograph (photo 7) the microstructure of the hot worked and annealed specimen is shown. Fig. 23 shows a logarithmic plot of the stress versus the steady state strain rate for two aluminum-zinc eutectoid specimens which had undergone the aforementioned treatments. We obtained part of the data from an Instron

machine and part from creep tests. The compatibility between the two techniques is very good considering that different specimens were used and that calibration errors exist in both procedures. The data revealed three different regions of different slope. Although the specimen which had not undergone the extra homogenization had a higher mean phase diameter, they showed faster deformation rates in all regions. Also, it can be noted from Fig. 23 that the superplastic region in the mechanically worked and recrystallized specimen extends over a wider range of strain rates. Consistent with the observations reported earlier, the low stress results from both thermal treatments revealed two distinct regions of constant n. At higher stresses n was found to be equal to 2 while below the subsuperplastic region n was found equal to 3. Another test was performed to study whether a second homogenization at 350°C and subsequent ice quence would have any effect on the steady state creep behavior of these alloys. Fig. 24 shows these results. Besides the variation due to the difference in the mean diameter no other effect due to the extra thermal treatment was observed.

In Fig. 24 we show the shear stress-shear strain plot of the two specimens deformed at a strain rate $5.23 \times 10^{-4}(\text{sec})^{-1}$ and at a temperature of 200°C. The maximum flow stress for the solution treated specimen was found to be higher to the mechanically worked and annealed specimen by a factor of 2.5. On the same figure we show the stress-strain behavior of a specimen which had been homogenized and furnace cooled to reveal the structure shown in photo 8. A marked difference in the microstructure appearance between photos 6, 7 and photo 8 can be seen. The slow cooling rate resulted in the characteristic eutectoid structure consisting of a plate like microstructure. The effect of this microstructure on the deformation strength of these alloys is remarkable. An almost tenfold increase

in the shear strength is shown in Fig. 25.

All of the above experiments were performed on double shear specimens. Tests were also conducted on tensile specimens. These experiments had the dual purpose 1) to study the strength characteristics of a tensile specimen and 2) to study the dependence of the total ductility on the thermomechanical history. The room temperature stress strain results are shown in Fig. 26. The maximum strengh of the two differently treated aluminum zinc alloys was the same. The mechanically worked and recrystallized specimen, however, reveals more ductility before failure. The furnace cooled alloy showed a relatively brittle behavior with an increase of the tensile strength of about 4000 psi. Tensile tests performed at 200°C revealed quite different results. Fig. 27 shows the stress strain curves for the furnace cooled specimens which were tested both at room temperature and at 200°C. The high temperature deformation produced more elongation, but the strength was reduced drastically. In Fig. 28, we show the stress strain curves of the deformed specimens with the two different thermomechanical histories. The solution treated specimen revealed a higher tensile strength, but less ductility. The amount of elongation, over 650%, exhibited by these specimens, is indicative of the superplastic mode of deformation which occurs at these strain rates and temperatures.

In photo 9 the failed specimens tested at room temperature are shown. The failure mode of the furnace cooled specimen is rather brittle, while the specimens with the globular fine microstructure failed after a considerable amount of necking. As shown in Fig. 26 the solution treated specimen exhibited less ductility than the hot worked and annealed specimen. In photo 10 we show the specimens tested at 200°C. Even at this high temperature the failure mode of the furnace cooled alloy is rather brittle not exhibiting any considerable amount of necking. The other two specimens

revealed extensive elongations, a characteristic feature of super-plastic deformation. In this temperature, too, the hot worked and annealed specimen revealed higher elongations than the solution treated one.

DISCUSSION

In the Results section we experimentally examined the validity of the assumptions made in the determination of the stress exponent value by the stress cycling technique. These assumptions are 1) that there are not microstructural changes during deformation which would affect the subsequent deformation at another load or strain rate and 2) that these materials behave like viscous fluids and do not exhibit any transient effects. Both of these assumptions were found to be invalid. A reproducible value of the stress exponent can be obtained by performing the minimal number of stress changes (or strain rate changes) on a single specimen in order to minimize the effect of the grain growth during deformation and by limiting the deformation to the minimum amount at each load (or strain rate) while making sure that the steady state is always achieved. In the literature investigators have attempted to correlate the stress exponent value to the amount of ductility after very large amounts of deformation. Because of the extended microstructural changes caused by these high elongations, these correlations are of dubious value. The technique we would like to suggest for the computation of the stress exponent is: to deform the specimen at the initial load (or strain rate) until steady state is clearly seen and then make small changes in the load or strain rate so as to minimize the transient effects and observe the new steady state. Also, by making small changes in the stress or strain rate one minimizes the possibility of computing the stress exponent between two points that correspond to different mechanisms.

A number of experimental results, reported by Bird, Murkherjee and Dorn (13), Vadiya, Murty and Dorn (36), Misro and Murkherjee (37) and

Alden and Schadler (22), showed that in a log $\dot{\varepsilon}$ versus log σ plot, a transition from an $n = 2$ region at higher stresses to an $n = 1$ region at lower stresses occurred for the Al-Zn superplastic alloy. This $n = 1$ value for the stress exponent at low stresses was attributed to a diffusional process. This diffusional process was supported by additional experimental evidence, such as the grain size dependence and the activation energy for creep, which is consistent with Coble's (35) model for the grain boundary diffusion creep. Diffusion has also been considered as the mass accommodating mechanism for the grain boundary sliding mechanism in the superplastic region. The results obtained from our studies revealed two distinct regions of constant n value. At the higher stresses the stress exponent was found to take the value 2, while at low stresses it took the value 3. Two different superplastic alloys, the Pb-Sn eutectic and the Al-Zn eutectoid alloys, were studied and revealed the same trend, that is, a transition from an $n = 2$ to an $n = 3$ region. All the identifiable thermomechanical treatments which could produce different microstructures and consequently influence the creep properties of these alloys were studied. The stress exponent results were found to be identical in all cases. Fig. 15 implies that the inconsistency between our results and those mentioned above is due to an experimental error involving extensive primary creep in this low stress region. It should be mentioned at this point that, while reports (13,22,36,37) show a transition from $n = 2$ to $n = 1$, our Fig. 16 shows a transition from $n = 3$ to $n = 1$. We feel confident about our results, as they are consistent with the results published by Mohammed and Langdon on Al-Zn eutectoid (50) and Pb-Sn eutectic (39), which showed a transition from $n = 2$ to $n = 4.1$ for Al-Zn and a transition from $n = 2$ to $n = 3$ for Pb-Sn. Most of this type of data reported

indicate a higher value for the stress exponent for the two extreme regions (10), in agreement with our findings. As was shown in the introduction, the smaller the value of n , the more elongations one expects. If indeed the stress exponent at the very low stresses was equal to 1 , then we would expect an even higher amount of superplastic deformation than in the $n = 2$ region. It has been reported though that neck free elongations correspond only to the $n = 2$ region and that superplasticity is limited at strain rates below the $n = 2$ region (11).

Samuelson and his coworkers (32) performed a very careful examination of the dislocation activity in a superplastic Al-Zn eutectoid alloy, deformed at strain rates corresponding to all three regions. Due to the experimental limitations, this study was performed on the aluminum rich grains only. The authors reported that the frequency of climbing dislocations decreased with the decreasing rate of deformation, while the number of gliding dislocations increases with the decreasing strain rates. If we would plot the ratio of the amount of climbing dislocation to the amount of gliding dislocation versus the strain rate of deformation, we would get Fig. 29. It can be seen that a straight line can pass through the experimental points. Fig. 29 also shows that around 2×10^{-5}/sec strain rate, the number of gliding dislocations is higher than the number of climbing dislocations. If we would assume that only these two mechanisms operate during the deformation of superplastic alloys, it would be expected that at higher strain rates dislocation climb will be the predominant mechanism, while at low stresses dislocation glide would control the deformation rate. These investigators also observed that the deformed specimens at low strain rates exhibited uneven distributions of the burgers vectors with fire slip planes operating

while for superplastic strain rates the deformed specimen showed more even distributions of the burgers# vector with six planes operating. The authors argued that the observations are pertinent to the deformation for anumber of reasons the strangest arguments being 1) the annealed specimen had a nonuniform distribution of burger's vectors than the deformed one and 2) the dislocation density and distribution observed did not change with strain.

The lead tin eutectic alloy consists of two solid solution phases: the lead rich phase and the tin rich phase. In the matrix of the lead rich phase, tin precipitates are dispersed. Weertman (56) proposed a model for the high temperature deformation of solid solution alloys over a rsnge of strain rates. He suggested that as the strain rate or stress is decreased, the predominant mechanism will evolve from dislocation climb to dislocation glide. In this lower stress mode, the dislocations cannot glide faster than the rate of solute atom diffusion. The activation energy for this deformation mechanism is expected to be equal to that of the activation energy for diffusion of the solute atom in the alloy. The stress exponent is expected to equal 3 for all alloys. Finally Weertman's formulation predicts a dependence of the strain rate on the solute concentration. This model has been verified for a number of alloys such as the Al-Mg, CuZn, Pb-Sn, and more. Both Wertman (54) and Murty (55) claimed the existence of such a mechanism in the Pb-Sn solid solution alloy. Unfortunately no extensive comparable data exist for the tin rich lead solid solution. In Table V we show the stress exponent activation energy for deformation for the low stress region of the three well-known superplastic alloys and the activation energy for diffusion of one component into the other. We see that the stress exponent in all three cases is equal to 3 and the activation

energy of deformation very close to that for the diffusion of one element into the matrix of the other. These results lead us to suggest that the low stress region in superplastic alloys is controlled by the viscous drag mechanism operating in the fastest deforming phase. This mechanism does not predict a grain size dependence, which has been reported repeatedly (5,39,11,20) for this low stress region. This grain size dependence, we believe, is an implicit parameter which is related to the composition of the two phases.

Experimental evidence support that the predominant mechanism in the $n = 3$ region is distinctly different than the predominant mechanism operating in the $n = 2$ region. Some of the observations supporting this point are:

(1) The difference of the stress exponent value in these two regions

(2) The difference in the deformation activation energy in the two regions. For superplastic deformation the activation energy is of the order of the activation energy for grain boundary diffusion while for deformation in the sub superplastic region the activation energy is of the order of the activation energy for diffusion in the bulk (51).

(3) The elimination of grain boundary sliding at low strain rates as measured by the surface scratch experiments (20).

(4) The grain elongation for deformation at strain rates corresponding to sub-superplastic region, although the microstructure remains globular for deformation at superplastic strain rates (10).

(5) Superplasticity is observed for deformation rates corresponding to the superplastic region but not the sub-superplastic region (11).

The present data suggest that the slowest deformation mechanism predominates the rate of deformation in the superplastic and subsuperplastic

region. This observation indicates that the two mechanisms operate in series, contrary to Murkherjee's proposition (29). He suggested that the low stress mechanism which was expected to be of the grain boundary diffusion type operates independently from the superplastic mechanism which involves the annihilation of dislocations at the grain boundary (1).

Now let us consider what kind of sequential mechanisms operate in Region I and Region II.

In view of a number of recent detailed studies involving both TEM and texture observations (23,24), we can comfortably assume that dislocations operate during the deformation of superplatic alloys at all strain rates. The observation reported by Samuelson et al. (32) that the dislocation density and distribution do not change to the annealed density and distribution even after extended amounts of deformation, suggests that dislocation activity may be closely related to the superplastic mechanism. As it was discussed in the introduction, it appears that a considerable amount of grain boundary sliding takes place during superplastic deformation. Theories have been developed which treat the material as a non Newtonian viscous fluid with a stress exponent equal to 2 (59). It is well established, however, that a number of microstructural changes takes place during superplastic deformation (9,12,22). These microstructural changes have led theorists to propose that although grain boundary sliding is taking place simultaneously and in series, mass movement occurs towards the triple points to relieve the Stress concentrations developed by the grain boundary movement. We would like to propose that superplastic deformation occurs via a grain boundary sliding mechanism and dislocation gliding occurs which contributes to the mass accomodation at the triple points.

When grain boundary sliding takes place points of stress concentration

are developed at the triple points. These stresses, which are random with respect to the direction of the applied stress, cause all six glide planes to operate. This is the reason why Samuelson et al. (32) observed a more uniform distribution of slip planes in the superplastically deformed specimen than the distribution revealed by the specimen deformed at low strain rates.

The question that we have to address now is: what it the criterion for the switch from dislocation glide at low stresses to grain boundary sliding at intermediate stresses in the rate controlling mechanism?

Hazzeldine et al. (25) argued that sliding may occur by the propagation of line defects through the grain boundary. Sliding on a regular smooth grain boundary is expected to be easy and arbitrary small stresses will cause sliding. Rel boundaries, though contain steps, ledges and other irregularities. The sliding rate is controlled by the elastic strain of the irregularities. At low stresses, the irregularities may anchor the grains and at progressively higher stresses, when the elastic strain of the irregularities is surpassed, the grains will be free to move.

Grain boundary sliding is expected only after a minimum amount of stress. Below this threshold stress, the grain boundaries might move against each other, but upon release of the load, the strains are recovered in time. This is what is known as anelastic strains, due to grain boundary movement. Zener (60) has proposed a model on how this may occur and Hart et al. (15) have incorporated this idea into their phenomenological deformation theories. If we assume that such a threshold stress exists, for deformations below this stress the grain boundaries are immobile and deformation takes place soleley by dislocation movement.

Asby and Verrall (28) justified the presence of a threshold stress on the basis of fluctuations in the grain boundary area. They estimated this threshold stress equal to $\frac{.72\Gamma}{d}$ where Γ is the grain boundary surface free energy and d is the mean grain size. For metals Γ varies from 100 erg/cm^2 to 1000 erg/cm^2 (61). If we take the smallest value of d equal to 1μm the treshold stress can be estimated to lie between .001 to .01 psi (49). This stress is far too low to account for the switch over in the predominant mechanism.

A second possibility is that the deformation rates of the two phases in the superplastic region are similar in magnitude. If grain boundary sliding occurs and the accomodation rate is similar on all sides of the triple point further sliding may occur. If, however, the accomodation rate is not compatible in both phases the grain boundary sliding will be limited and the rate controlling mechanism would be the dislocation gliding in the fastest deforming phase.

In the Results section we reported that the rate of deformation of a lead tin eutectic specimen depends greatly on its thermomechanical history. Specimens made from the more voluminous ingot resulted in higher strain rates. Variations in the amount of mechanical working did not appear to have an effect on the deformation rate of these alloys, although a certain amount of mechanical working prior to testing is required for superplasticity. We also reported that the ingots of different dimensions revealed different microstructures in that, for the same mean phase diameter, different lead rich mean phase diameters may be obtained. If we make the assumption that statistically the line fraction as derived from the mean phase intercept is directly related to the volume fraction, then we can estimate the volume fraction of the lead rich phase in each ingot as

$$V_{Pb} = \frac{L_b}{L_{Pb} + L_{Sn}} = \frac{2L_{Pb}}{d} \qquad \text{Equation 10}$$

Applying this equation to the data reported in Fig. 17 we obtain the volume fraction of the lead rich phase for specimen 1A as .27, while for specimen 2A it is estimated as .30. In Table IV we show the volume fraction of the lead rich phase together with the resulting A values, as discussed previously. A direct correlation between the volume fraction of the lead rich phase and A can be seen. The higher the volume fraction of the lead rich phase, the slower the strain rate. It can also be said that the slower cooled alloy possesses the composition most closely related to the room temperature equilibrium composition. The lead rich phase has a much higher concentration of tin which should precipitate out. In the same table we show some other reported results to substantiate this point. Beutelet and Suery (68) have reported the mean lead rich phase diameter and the mean phase diameter for a lead tin eutectic alloy. Their cast was .8 inches in diameter and the lead rich volume fraction is estimated as .36. While reanalyzing some old data (51), we find that they are well in line with the results we report here. Mohammed and Langdon's (39) results, which were obtained on a two inch ingot, revealed an A value of around 1050, which again is in line with what would be expected from our results.

The dependence of the strain rate on the relative amounts of each phase has been demonstrated by Herriot et al. on the copper phosphorous alloy. Herriot et al. (57) reported that the strain rate is dependent on the phosphorous concentration and that a microstructure characterization parameter of the for $La(La + Lb)^2$ would represent the data well. This

representation was applied to our data but was found inadequate to scale the data to a single line. An attempt to find a relationship between the A value and the volume fraction was not successful, because of the close range of volume fractions observed and the experimental errors.

In superplasticity the stress and microstructure exponents are generally agreed upon but the pre-exponential value varies between investigations. This variation in the A value could very well be due to the different thermomechanical histories of the specimens in the various investigations. Also, comparisons between theoretical models and experiment is dubious because none of these models take into consideration the effect of the variation of the lead rich phase due to the thermomechanical history on the strain rate.

The influence of the thermomechanical history on some of the mechanical properties of the Al-Zn eutectoid alloy was also studied. It was found that the hot worked alloy exhibited higher elongations and lower flow stresses at 200°C than the one which was solution treated and fast quenched. The room temperature deformation seems to be unaffected by such a treatment, although the solution treated specimen revealed less ductility. The fine microstructure required for superplasticity can be altered to a lamellar type of microstructure by a slow cooling rate. This change in the microstructural appearance can increase the flow strength of the alloy by a factor of more than 6 at high temperature. Although the room temperature strength is also increased by this new microstructure, it does not compare with the improvement at the higher temperatures, where the superplastic mode of deformation is suppressed.

The strengthening mechanism proposed here can only be applied to components made of alloys of eutectoid composition. Most of the com-

mercially available or comercially interesting superplastic alloys such as the Al-Zn, the titanium-aluminum, the high carbon steets are made of eutectoid or near eutectoid compositions. Of course this extra thermal treatment would mean an additional cost. Whether this additional manufacturing cost is economically advantageous we leave up to the industrialist to decide.

SUMMARY

(1) During superplastic deformation there is a considerable amount of grain growth resulting from both the high testing temperature and the deformation itself. Deforamtion at superplastic and sub-superplastic strain rates reveal transient effects. These two observations have to be considered when computing the stress exponent value.

(2) The stress exponent value at the low stress region was found equal to 3 and not equal to 1 as reported elsewhere. This inconsistency was suggested to be due to the extensive primary creep observed in these alloys at the low stresses. The experimental observations such as the stress exponent equal to 3 and the activation energy for creep in the neighborhood of that for diffusion of the solute atom in the matrix bear close resemblance to the solute drag deformation mechanism proposed by Weertman.

(3) The thermomechanical history of a specimen has a great effect on the creep properties of alloys. These thermomechanical treatments are believed to have an effect on volume fraction of each of the two phases.

(4) The strength of a eutectoid alloy superplastically deformed can be drastically increased by an additional thermal treatment which consists of homogenizing the deformed part in the single phase and then slow cooling to induce the typical eutectoid structure.

ACKNOWLEDGMENT

The author would like to thank Professor J.W. Morris, Jr. for his guidance throughout this work. This work was done under the auspices of the U.S. Department of Energy.

APPENDIX

The quantities appearing in equation (1) are defined as follows:

$\dot{\gamma}$ = strain rate

k = Boltzman's constant

T = absolute temperature

D_o = a characteristic diffusivity, chosen equal to the pre-exponential D_o in the diffusion equation for pure Sn, $(.08\ cm^2/sec)$[15].

G = a characteristic stress, taken equal to the shear modulus of pure Sn, $(2 \times 10^{11} Id/cm^2))$[15].

τ = resolved shear stress

d = mean grain diameter

REFERENCES

1. C.E. Pearson, J. Inst. Met. 54, 111 (1934).

2. W. Rosenhaim, J.L. Haughton, K.E. Bingham, J. Int. Metals 23, 261 (1920).

3. A.A. Bochvor, Z.A. Sviderskain, Izv Akad Nauk SSSR Otdel Tekn Nauk 9, 851 (1945).

4. E.E. Underwood, J. Metals 14, 914 (1962).

5. Metals and Materials, April 1970, page 142 (1975) 569.

6. O.D. Sherby, B. Walser, C.M. Yoting, E.M. Cady, Scripta Met 9, 597.

7. E.W. Weisert, G.W. Stacher, Metal Progress 111, 32 (1977).

8. G.J. Davies, J.W. Edington, C.P. Cutler, K.A. Padmayabhaum, J. of Mat. Sci. 5, 1091 (1970).

9. W.A. Backofen, I.R. Turner and D.H. Avery, ASM Quar. Tran. 57, 980 (1964).

10. R.H. Johnson, Metallurgical Reviews No. 146, 115 (1970).

11. F.A. Mohamed, M. Mahmed and T.G. Langdon, Met Trans. 8, 933 (1977).

12. S.W. Zehr, W.A. Backofen Trans. ASM 61, 300 (1968).

13. J.E. Bird, A.K. Mukherjee, J.F. Dorn. "Quantitative Relation Between Properties and Microstructure," Israel University Press (1969), p. 255

14. H.W. Hayden, R.C. Gibson, H.F. Merrick, J.F. Brophy Trans Amer Soc Metals 60, 3 (1967).

15. E.W. Hart, C.Y. Li, H. Yamada, G.L. Wire, Constitutive Equations in Plasticity, Chap. 5, p. 149. A.S. Argon ed. MIT Press, Cambridge (1975).

16. E.W. Hart, Acta Met 18, 599 (1970).

17. J. Hedworth, M.J. Stonewell, J. of Mat. Sci. 6, 1061 (1971).

18. A.E. Geckinli, C.R. Barret, J. of Mat. Sci. 11, 510 (1976).

19. T.H. Alden, Acta Met 15, 469 (1967).

20. D. Lee, Acta Met 17, 1057 (1969).

21. A. Ball, M.M. Hutchison, Metas. Sci. J. 3, 1 (1969).

22. J.H. Alden, H.W. Schadler, Trans of AIME 242, 825 (1968).

23. H. Nazizi, R. Pearce, Scripta Met. 3 807 (1969).

24. G.P. Cutler, J.W. Edington, Metals Sci. J. 5, 201 (1971).

25. P.M. Hazzledine and D.E. Newbury, In Grain Boundary Structure and Properties, edited by G.A. Chadwick and D.A. Smith Academic Press (1976), Chap. 7, p. 235.

26. R.B. Jones, Nature 207 70 (1965).

27. D.H. Avery, W.A. Backofen, Trans. Quart. ASM 58, 551 (1965).

28. F.M. Asby, R.A. Verral, Acta Met 21, 199 (1973).

29. A.K. Mukherjee, Mat. Sci. Eng. 8, 83 (1971).

30. R.B. Nicholson, Proceedings of the International Materials Symposium, University of California (1972).

31. D.L. Holt, Trans. Met. Soc. AIME 242, 85 (1968).

32. L.C. Samuelson, K.N. Melton, J.W. Edington, Acta Met 24, 1017, (1976).

33. Y. Kobayashi, Y. Ishida, M. Kato, Scripta Met 9, 51 (1977).

34. H. Naziri, R. Pearch, M. Henderson, Brown, K.F. Hale, Acta Met. 23, 489 (1975).

35. R,K, Coble, J. Appl. Phys. 34, 1679 (1963).

36. M.L. Vadiya, K.L. Murty, J.E. Dorn, Acta Met. 21, 1615 (1973).

37. S. Misro, A. Mukherjee, Rate Processes in Plastic Deformation of Materials Proc. J. E. Dorn Symposium, American Society for Metals, Cleveland, Ohio (1975).

38. D. Grivas, J.W. Morris, LBL Report 2532 (1973).

39. F.A. Mohamed, T.G. Langdon, Phil Mag 32, 697 (1975).

40. H. Naziri, P. Pearce, J. Inst. Metals 97, 326 (1969).

41. W.B. Morrison, Trans ASM 61, 923 (1968).

42. W.B. Morrison, Trans. Met. Soc. AIME 242, 2221 (1968).

43. W.A. Tiller, R. MrDjenovich, J. of Applied Phys. 34, 3639 (1963).

44. D. Turnball and H.N. Treaftis, Acta Met. 3, 43 (1955).

45. R.H. Johnson, G.M. Packer, L. Anderson, O.D. Sherby, Phil Mag 18, 1309 (1963).

46. D.I. Holt and W.A. Backofen Trans AIME 59, 755 L(1966).

47. M.J. Stonewell, J.L. Roberson, B.M. Watts, Mat Sci. J 3, 41 (1969).

48. B.M. Watts, M.J. Stonewell, Mat. Sci. J. 6, 228 (1971).

49. G. Raj, N.J. Grant, Met. Trans 6A, 385 (1975).

50. F.A. Mohamed, T.G. Langdon, Acta Met 23, 117 (1975).

51. D. Grivas, MSE Thesis, LBL 2547 (1974).

52. J.E. Hilliard, Metal Prog. 85, 99 (1964).

53. Y.C. Li, Private communication.

54. J. Weertman, Trans. AIME 218, 207 (1960).

55. K.L. Murty, Mat. Si. and Eng. 14, 169 (1974).

56. B. Baudelet, M. Suery, J. Mat. Sci. 7, 512 (1972).

57. G. Herriot, B. Bandelet, J. Jonas, Acta Met. 24, 689, (1976).

58. R.C. Gifkins, Met. Trans. 7A, 1225 (1976).

59. K.A. Padmanabham, Mat. Sci. and Eng. 29, 1 (1977).

60. C.M. Zener, Elasticity and Anelasticity of Metals, University of Chicago Press (1948).

61. J.P. Hirth, J. Lothe, Theory of dislocations. McGraw Hill Book Company, New York (1968).

TABLE I

Specimen	Composition	
1A	Pb-62Sn	2 inch diameter ingot, reduced to 7/8 inch rod at R.T.
1B		machined to 1 inch rod, and reduced to 7/8 inch rod at R.T.
1C		machined to 1 inch rod, and reduced to 7/8 inch rod at R.T.
2A		1 inch diameter ingot, reduced to 7/8 inch rod.
2B		machined to 1 inch rod, and reduced to 7/8 inch rod at R.T.
3A		1 inch diameter ingot, reduced to 7/8 inch rod.
4A	Al-22Zn	1 inch diameter ingot, reduced to 7/8 inch rod at 350°C.
4B		As 4A plus asolution treatment at 350°C for 20 hours and ice quench.
5A		As 4A and rolled to 1/8 inch plate at 260°C.
5B		As 5A plus a solution treatment at 350°C for 20 hours and ice quench.

TABLE II

Cross section	Initial mean phase diameter				17.5μm	Final mean phase diameter				22μm
Longitudinal	"	"	"	"	20.7μm	"	"	"	"	23μm

TABLE III

Initial mean phase diameter	Final mean phase diameter of crept specimen at 214°C	Final mean phase diameter of crept specimen at 208°C
1.1μm	2.2μm	2.9μm

TABLE IV

Volume fraction of Pb rich phase		A	Cast Diameter
.238	at Room Temperature		
.315	" Eutectic 11		
.27	From Specimen 1A	2000	2"
.30	Specimen 2A	800	1 "
.32	Specimen 3A	100	1
.34	Grivas, Murty, Morris	100,200	1
.36 to .44	Beatelet & Suvey		.8
	Grivas, Morris	5000	2 "
?			tension
?	Mohamad & Langdon	1050	2"

TABLE V

	n	ΔH deformation (kcal/mole)	ΔH diffusion (kcal/mole)	
Alloy	Region I	Region I		
Sm-38Pb	3	18.9 20.1	Sm in Pb	18.5
Al-22Zn	3	26.5 20.0	Al in Zn	27
Al-68Mg	3	30.5	Al in Mg	31.5

FIGURE CAPTIONS

Fig. 1. The strain rate exponent m (inverse of the stress exponent n used in this thesis) versus the strain rate for the head tin eutectic alloy. Zehr and Backofen (12)

Fig. 2. Experimental methods used in studying the plastic deformation of materials.

Fig. 3. Schematic load-elongation curve of a velocity change test for the computation of the stress component.

Fig. 4. The dimensions of the double shear and tensile specimens used in this investigation.

Fig. 5. Creep test apparatus.

Fig. 6. Schematic drawing of the apparatus used to conduct tensile tests.

Fig. 7. Logarithmic steady state shear strain rate versus the applied shear stress showing a slope near to 2 and the effect of previous straining on the strain rate.

Fig. 8. Typical creep curve for the superplastic deformation of Pb-Sn eutectic with the anelastic strain on the same figure.

Fig. 9. Work hardening and work softening for deformation rates corresponding to the superplastic region.

Fig. 10. Results from the stress relaxation test on the Pb-Sn eutectic alloy.

Fig. 11. Steady state shear strain rate versus the applied stress plot for the Al-Zn eutectoid alloy showing the effect of the loading history and the transition from and m=2 region to n=3 at lower stresses.

Fig. 12. Logarithmic plot of the steady state shear strain rate versus the applied stress for the Pb-Sn eutectic alloy showing the effect of the microstructural changes during deformation on the strain rate.

Fig. 13. Creep curve for Pb-Sn eutectic alloy deformed at a stress corresponding to the sub-superplastic region.

Fig. 14. Creep curve of an Al-Zn eutectoid alloy deformed at a stress corresponding to the n=3 region, showing an extensive amount of primary creep.

Fig. 15. A double log plot of the steady state shear strain rate versus the applied stress at low stresses exhibiting a stress exponent equal to 3.

Fig. 16. A double log plot of the shear strain rate versus the applied stress after approximately 5% strain at each load.

Fig. 17. Double log plot of the mean phase diameter vs the annealing time for the Pb-Sn eutectic alloy.

Fig. 18. Arrhenius plot of the logarithmic mean phase diameter versus 1000/T for the computation of the activation energy for phase growth.

Fig. 19. Plot of mean phase diameter versus the mean lead rich phase diameter, indicating that for the same mean phase diameter value there may exist two different values of the mean rich phase diameter.

Fig. 20. Double log plot of the steady state strain rate versus the applied stress for the Pb-Sn eutectic alloy prepared from two different ingots.

Fig. 21. Creep data in the form of equation 4.
▽ d = 6.31.2μm □d = 5.5 ± .3μm ■d = 6.2 ± .3μm ◇d = 4.2 ± .3μm
◆5.4 ± .2μm

Fig. 22. Creep data of Pb-Sn eutectic presented in the form of equation 4.
□d = 4.61 ± .3μm △ d = 5.51.4μm ● as in Fig. 20
▲d = 4.7 ± .3μm

Fig. 23. Double log plot of the steady state shear strain rate versus the shear stress for the Al-Zn eutectoid alloy which had undergone different thermomechanical treatments.

Fig. 24. Double log plot of the steady state shear strain rate versus the shear stress to check the possible effect of a second homogenization and ice quench on the deformation rate of this alloy.

Fig. 25. The shear stress versus the shear strain for the Al-Zn eutectoid specimens which had undergone different thermal treatments.

Fig. 26. Tensile stress versus strain plot for the Al-Zn specimens tested at room temperature.

Fig. 27. Tensile stress versus tensile strain plot for the furnace cooled Al-Zn eutectoid specimens at R. T. and 200°C.

Fig. 28. Tensile stress versus tensile strain of two Al-Zn eutectoid specimens tested at 200°C.

Fig. 29. A reanalysis of Samuelson's data showing the increasing ratio of the number of gliding dislocations over the number of climbing dislocations as the strain rate is decreased.

PHOTOGRAPH CAPTIONS

Photo 1. a, b typical microstructures of specimens 1A, typical microstructures of specimens 1A (a,b) and 2A (c,b) after 120 hours of arnealing at 170°C. 700x

Photo 2. Microstructure of Pb-Sn eutectic alloy showing the Sn precipitates. 2500x

Photo 3. SEM photo of the Pb-Sn eutectic alloy including the x-ray analysis. 3750x

Photo 4. The microstructure of the Pb-Sn eutectic alloy showing the tin grains. 1600x

Photo 5. Microstructure of as cast Pb-Sn eutectic alloy after 94 days at room temperature. a) 1500x, b) 2000x

Photo 6. Microstructure of the homogenized and quenched Al-Zn eutectoid alloy. a) 2500x, b) 1500x

Photo 7. Microstructure of worked and annealed Al-Zn eutectoid specimens. 2500x

Photo 8. Microstructure of the furnace cooled Al-Zn eutectoid alloy. 2000x

Photo 9. Failed Al-Zn eutectoid specimens tested at room temperature. a) furnace cooled, b) solutions treated and ice quenched c) worked and annealed.

Photo 10. Failed Al-Zn eutectoid specimens tested at 200°C. a) furnace cooled, b) solution treated and ice quenched, c) worked and annealed.

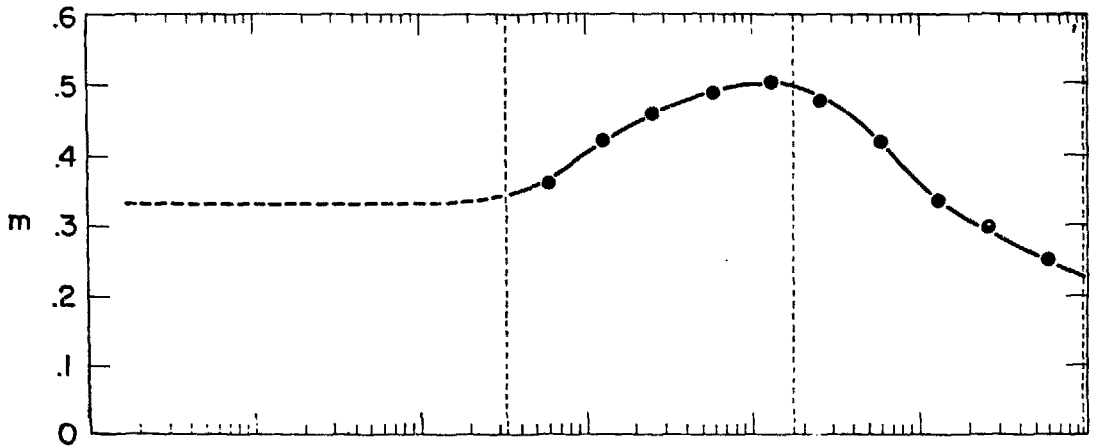

Fig. 1

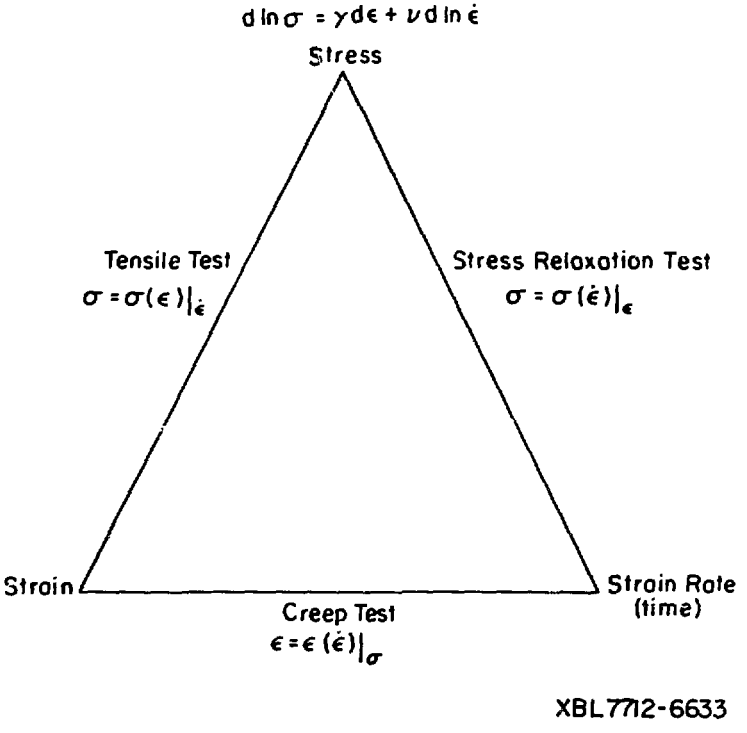
$d \ln \sigma = \gamma d\epsilon + \nu d \ln \dot{\epsilon}$
Stress
Tensile Test
$\sigma = \sigma(\epsilon)|_{\dot{\epsilon}}$
Stress Relaxation Test
$\sigma = \sigma(\dot{\epsilon})|_{\epsilon}$
Strain
Strain Rate
(time)
Creep Test
$\epsilon = \epsilon(\dot{\epsilon})|_{\sigma}$
XBL7712-6633

Fig. 2

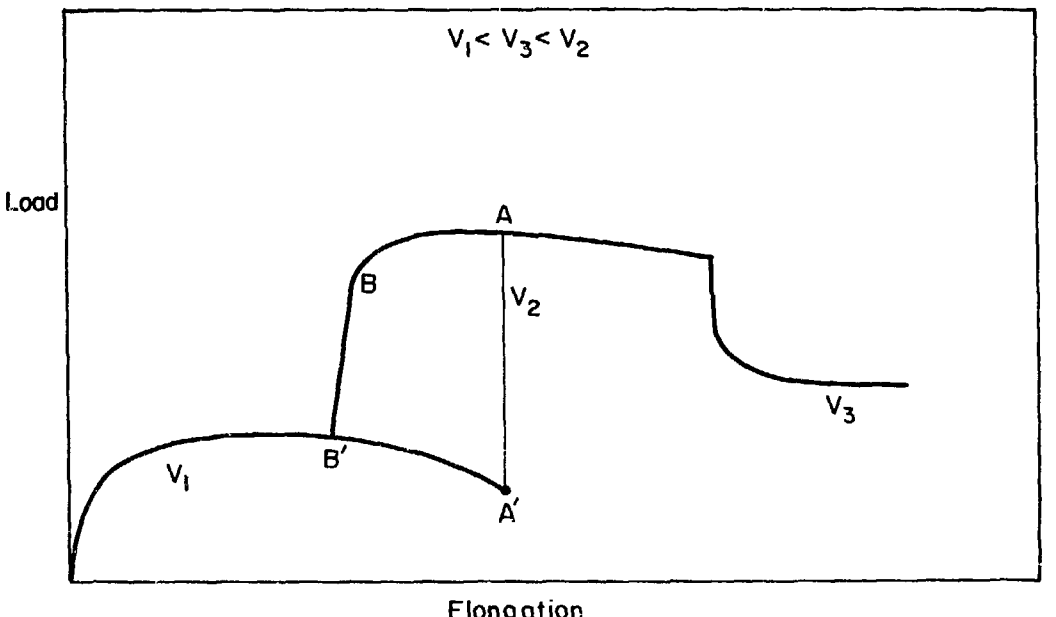

XBL 7712-6648

Fig. 3

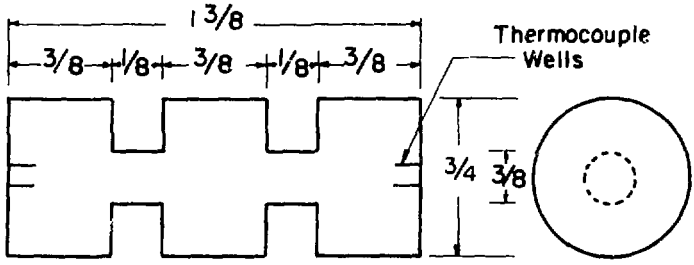

Double Shear Specimen

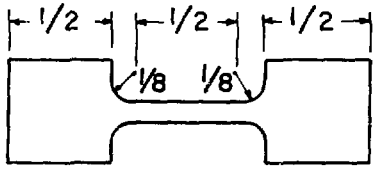

Tensile Specimen
Thickness = 1/16"

XBL7712-6643

Fig. 4

CREEP MACHINE

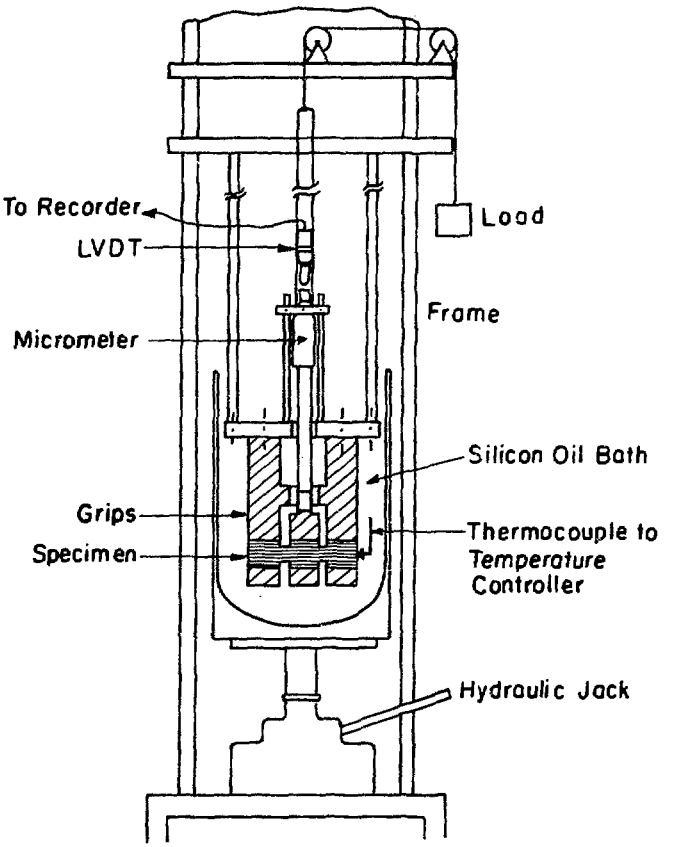

Fig. 5

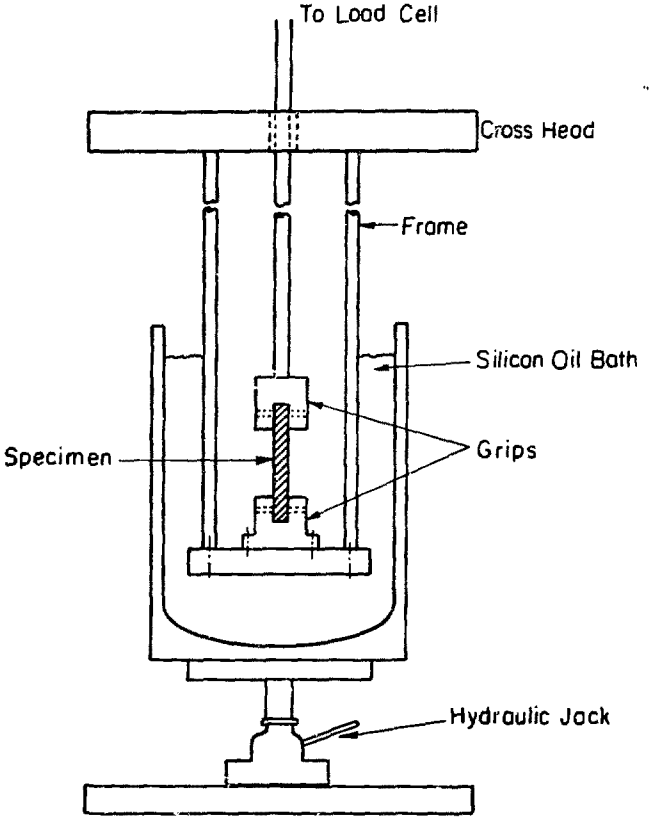
To Load Cell
Cross Head
Frame
Silicon Oil Bath
Specimen
Grips
Hydraulic Jack
XBL7712-6644

Fig. 6

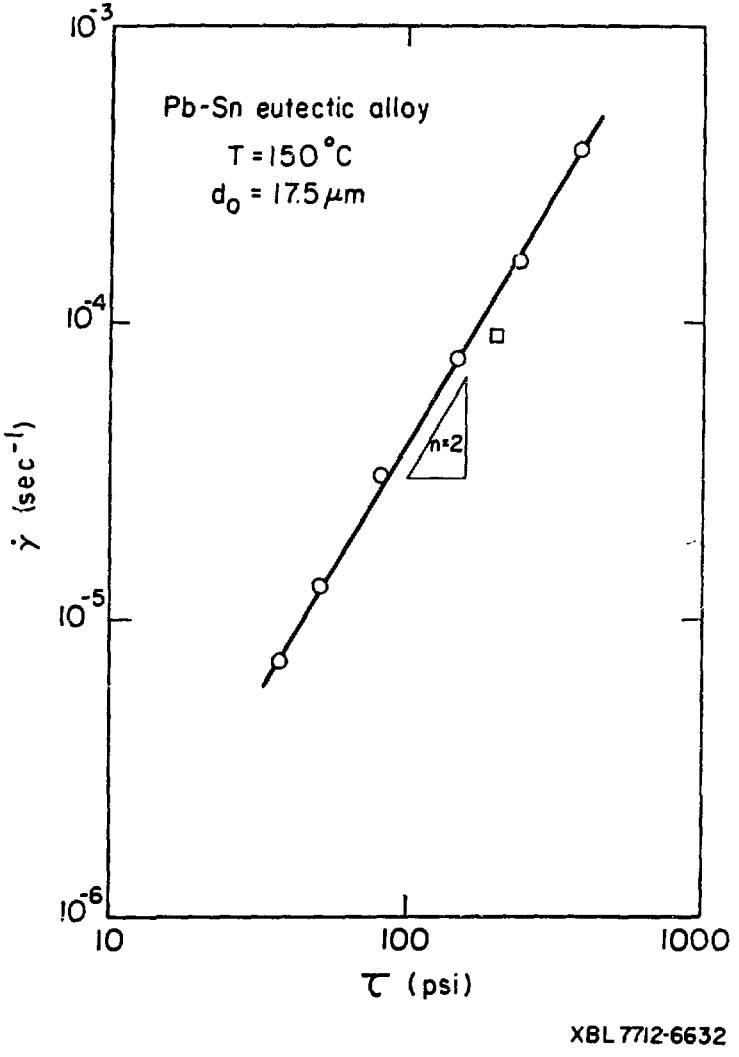
Pb-Sn eutectic alloy
T = 150 °C
d_0 = 17.5 μm
n=2
$\dot{\gamma}$ (sec^{-1})
10^{-3}
10^{-4}
10^{-5}
10^{-6}
10
100
1000
τ (psi)
XBL 7712-6632

Fig. 7

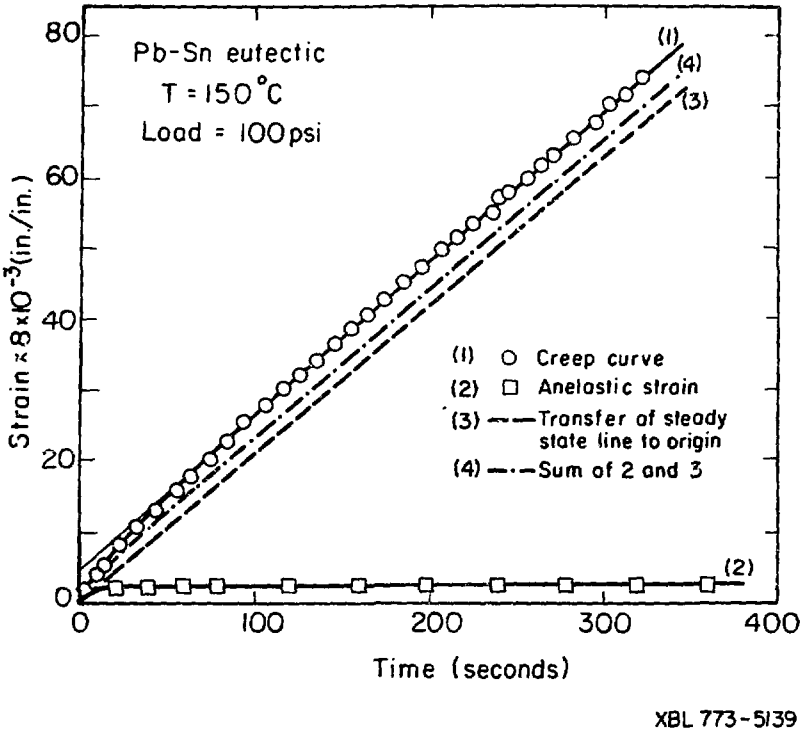

XBL 773-5139

Fig. 8

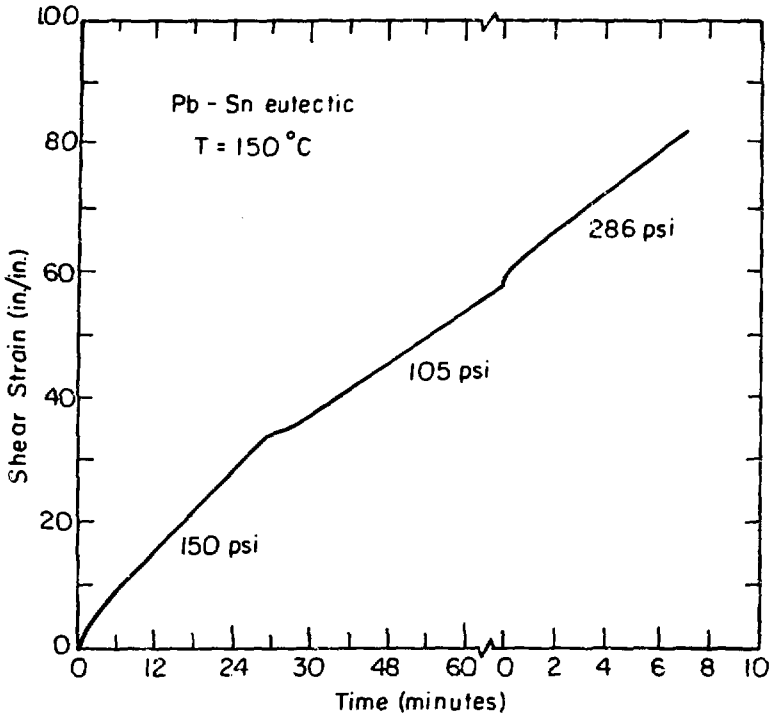

XBL 7712-6649

Fig. 9

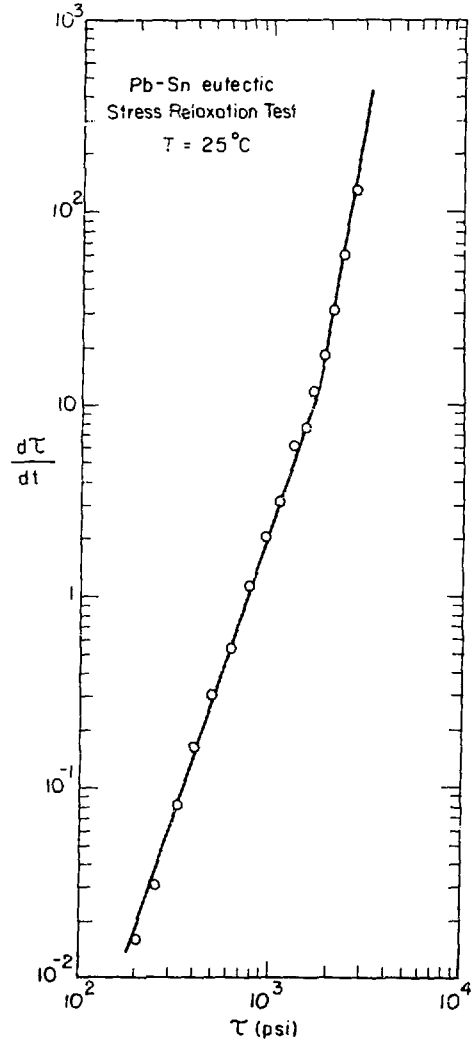
Pb-Sn eutectic
Stress Relaxation Test
T = 25°C
10^3
10^2
10
1
10^{-1}
10^{-2}
$\frac{d\tau}{dt}$
10^2
10^3
10^4
τ (psi)
XBL782-4572

Fig. 10

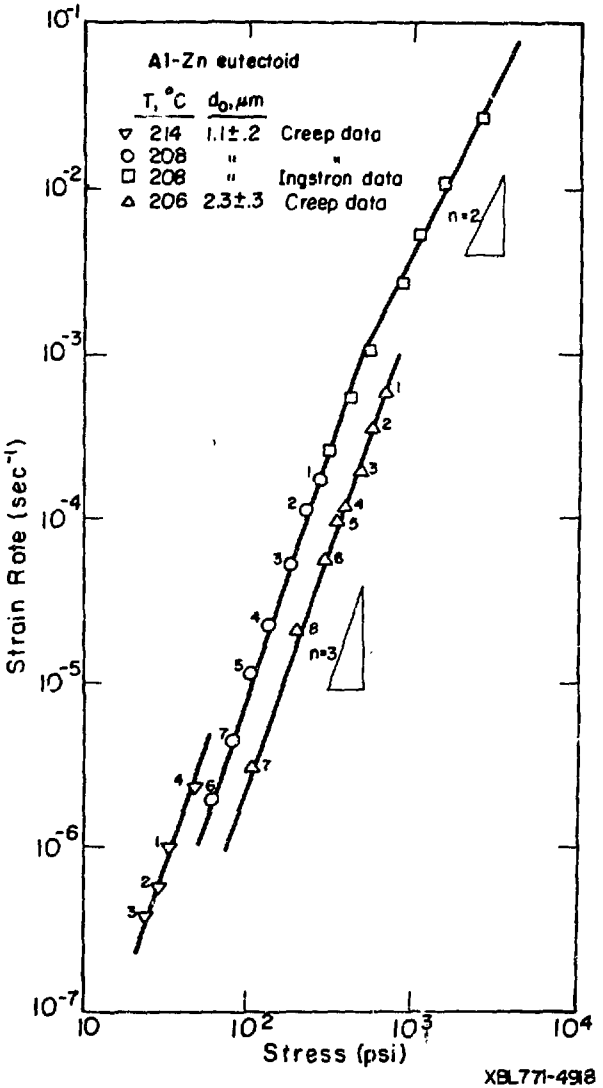
Al-Zn eutectoid
T, °C
d₀, μm
214
1.1±.2
Creep data
208
"
"
208
"
Ingstron data
206
2.3±.3
Creep data
n=2
n=3
Strain Rate (sec⁻¹)
Stress (psi)
XBL771-4918

Fig. 11

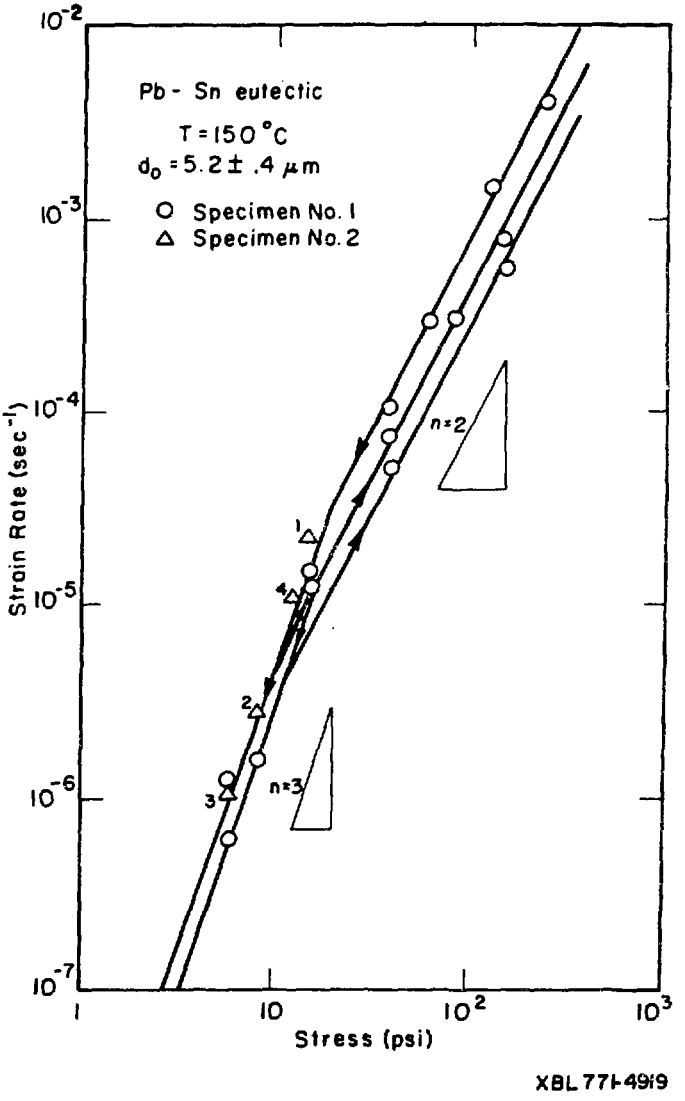
Pb - Sn eutectic
T = 150 °C
d_0 = 5.2 ± .4 μm
O Specimen No. 1
Δ Specimen No. 2
n=2
n=3
1
2
3
4
Strain Rate (sec^{-1})
Stress (psi)
10^{-2}
10^{-3}
10^{-4}
10^{-5}
10^{-6}
10^{-7}
1
10
10^2
10^3
XBL 771-4919

Fig. 12

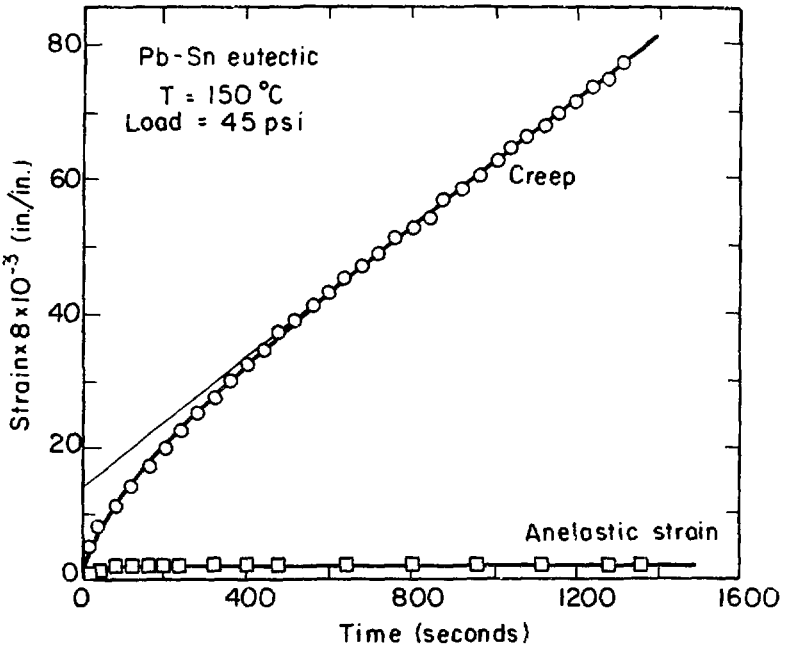

XBL 773-5140

Fig. 13

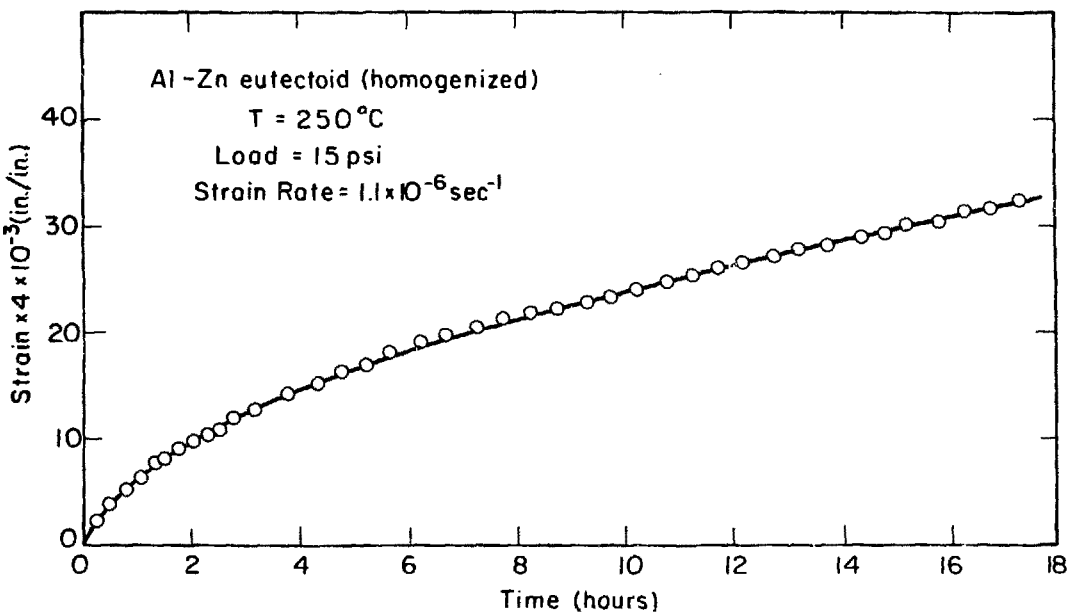

XBL 773-5142

Fig. 14

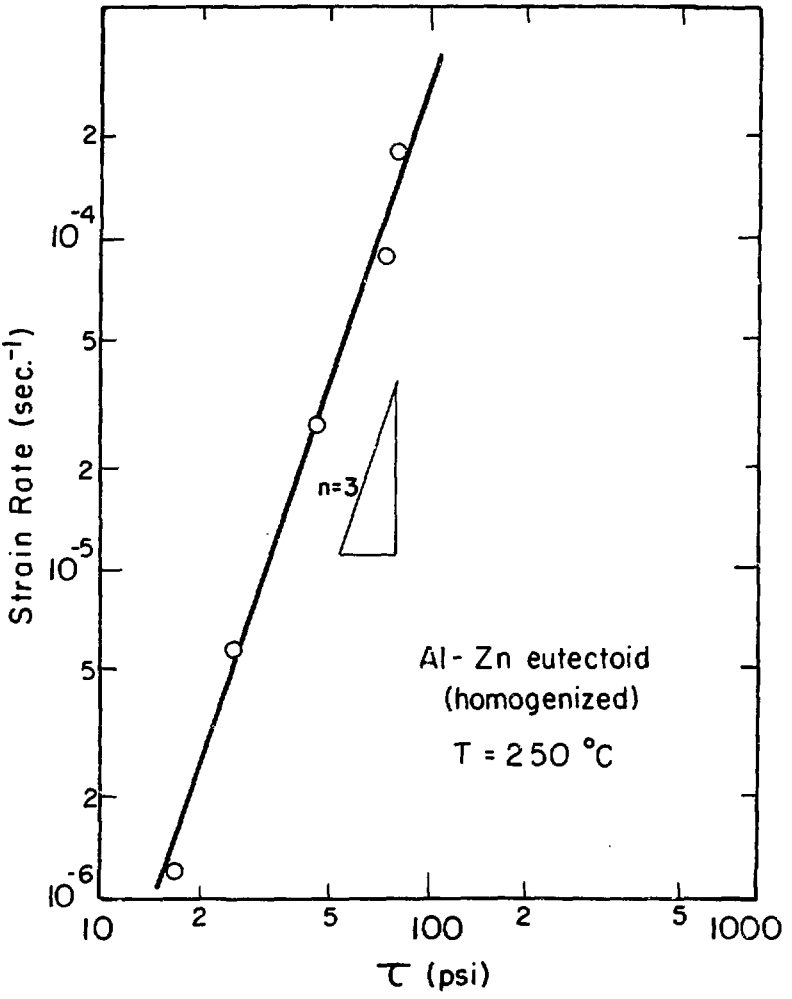
Strain Rate (sec.$^{-1}$)
10^{-4}
10^{-5}
10^{-6}
2
5
n=3
Al - Zn eutectoid
(homogenized)
T = 250 °C
10
100
1000
τ (psi)
XBL 773-5141

Fig. 15

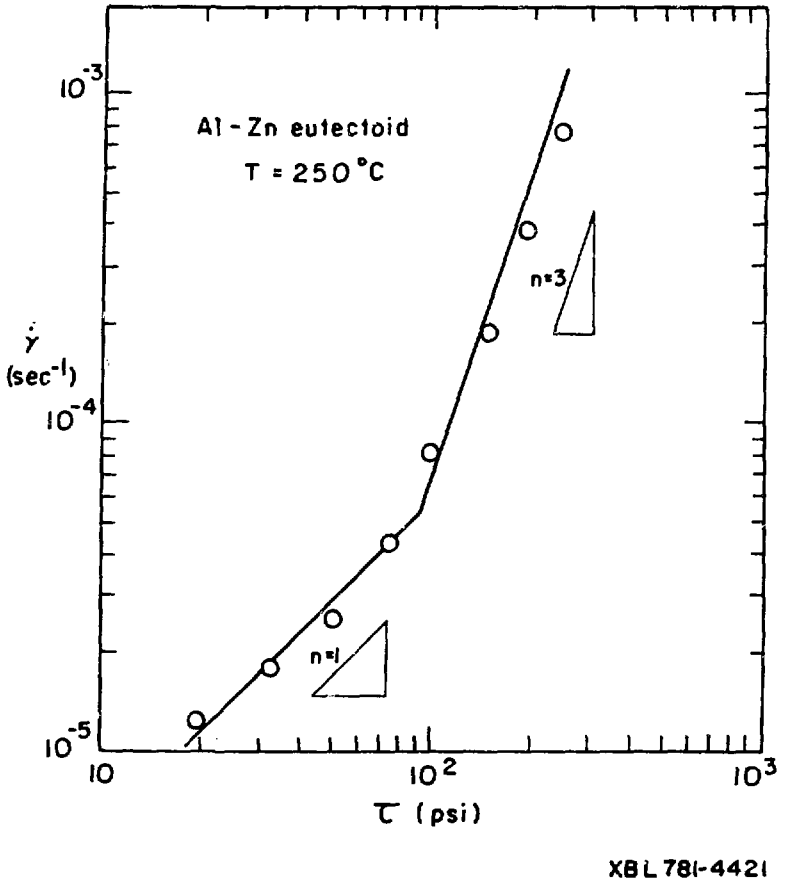
Al - Zn eutectoid
T = 250 °C
n=3
n=1
$\dot{\gamma}$ (sec^{-1})
10^{-3}
10^{-4}
10^{-5}
10
10^2
10^3
τ (psi)
XBL 781-4421

Fig. 16

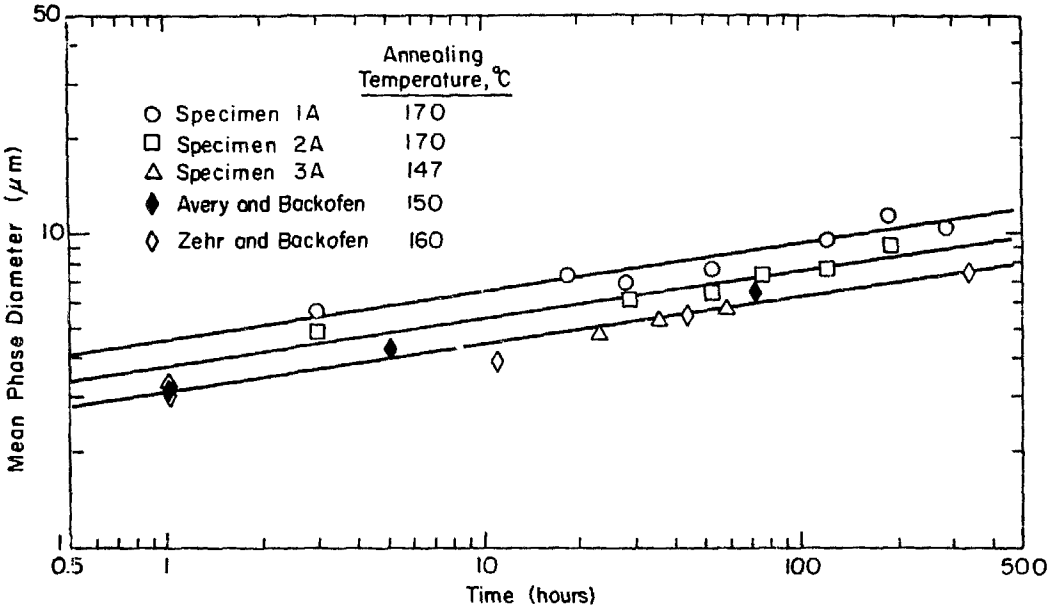
50
10
1
Mean Phase Diameter (μm)
0.5
1
10
100
500
Time (hours)
Annealing Temperature, °C
Specimen 1A 170
Specimen 2A 170
Specimen 3A 147
Avery and Backofen 150
Zehr and Backofen 160
XBL7712-6642

Fig. 17

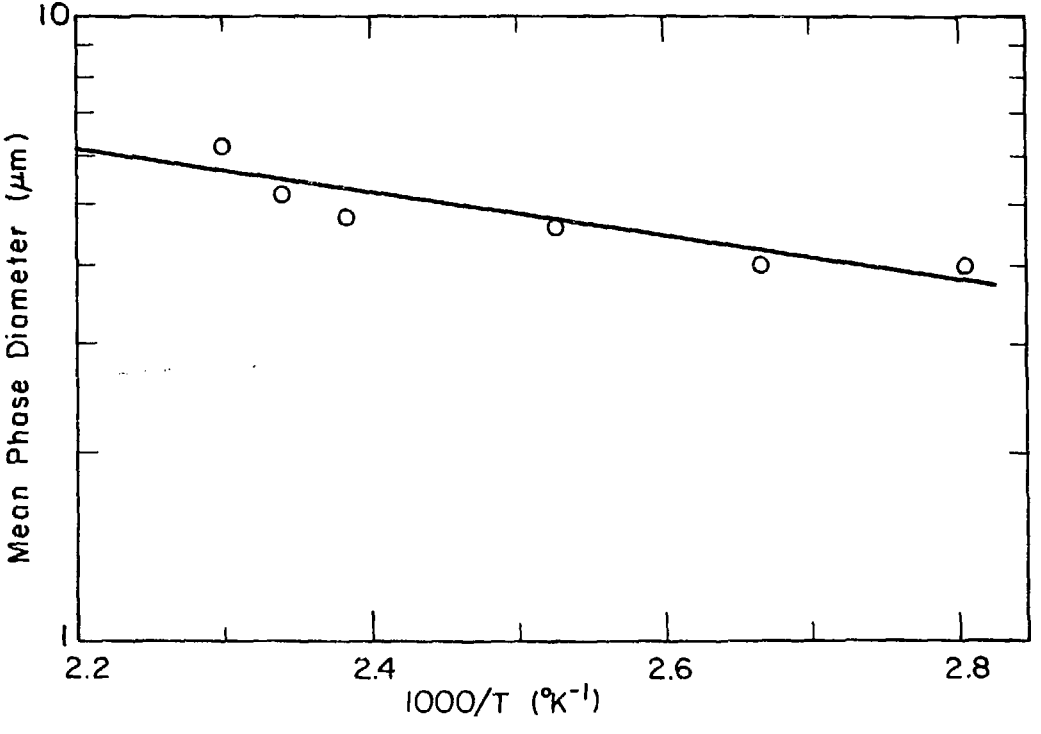

Fig. 18

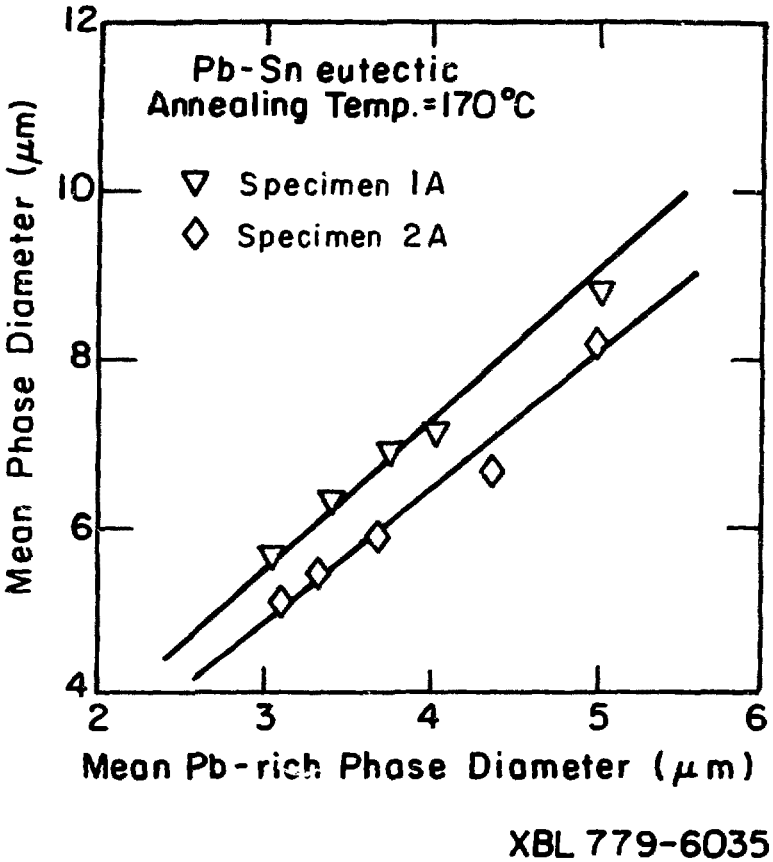
Pb-Sn eutectic
Annealing Temp.=170°C
Specimen 1A
Specimen 2A
Mean Phase Diameter (μm)
Mean Pb-rich Phase Diameter (μm)
12
10
8
6
4
2
3
4
5
6
XBL 779-6035

Fig. 19

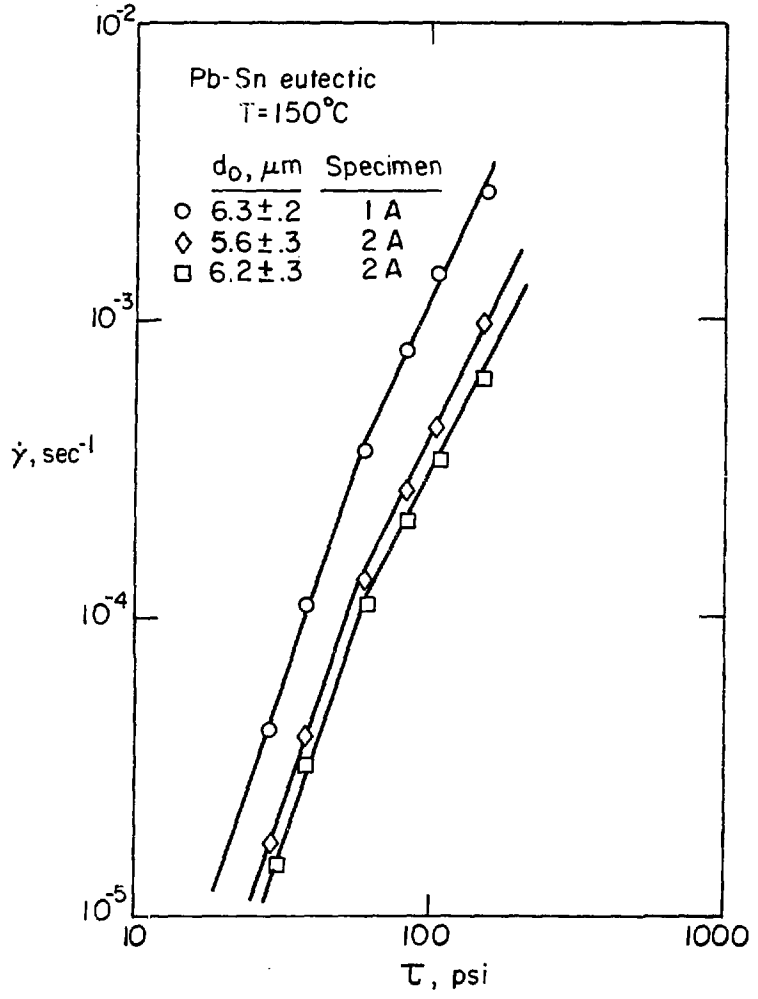
Pb-Sn eutectic
T=150°C
d0, μm Specimen
○ 6.3±.2 1 A
◇ 5.6±.3 2 A
□ 6.2±.3 2 A
10-2
10-3
10-4
10-5
γ̇, sec-1
10
100
1000
τ, psi
XBL 772-5123

Fig. 20

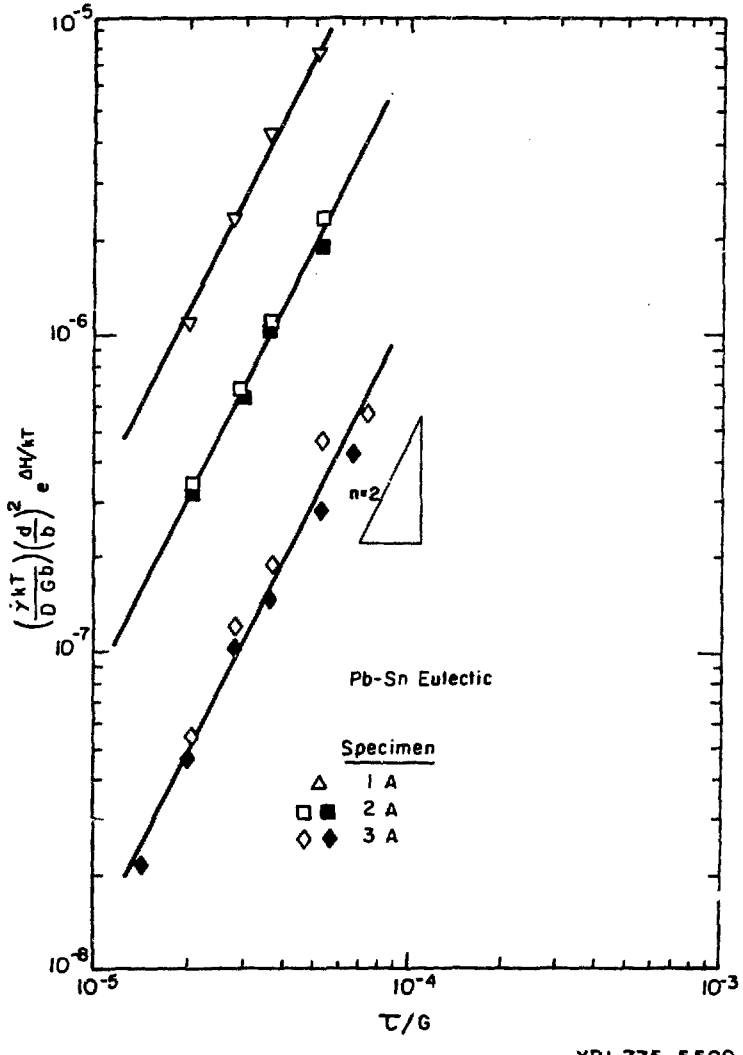
10^{-5}
10^{-6}
10^{-7}
10^{-8}
$\left(\frac{\dot{\gamma} kT}{D Gb}\right)\left(\frac{d}{b}\right)^2 e^{\Delta H/kT}$
n=2
Pb-Sn Eutectic
Specimen
1 A
2 A
3 A
10^{-5}
10^{-4}
10^{-3}
τ/G
XBL775-5509

Fig. 21

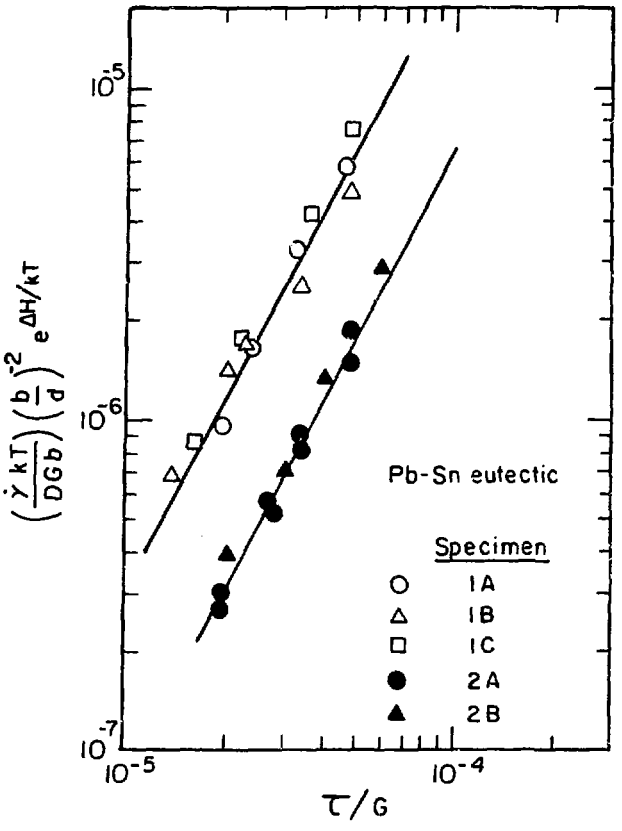
$\left(\frac{\dot{\gamma} kT}{DGb}\right)\left(\frac{b}{d}\right)^{-2} e^{\Delta H/kT}$
10^{-5}
10^{-6}
10^{-7}
10^{-5}
10^{-4}
τ/G
Pb-Sn eutectic
Specimen
1A
1B
1C
2A
2B
XBL781-4422

Fig. 22

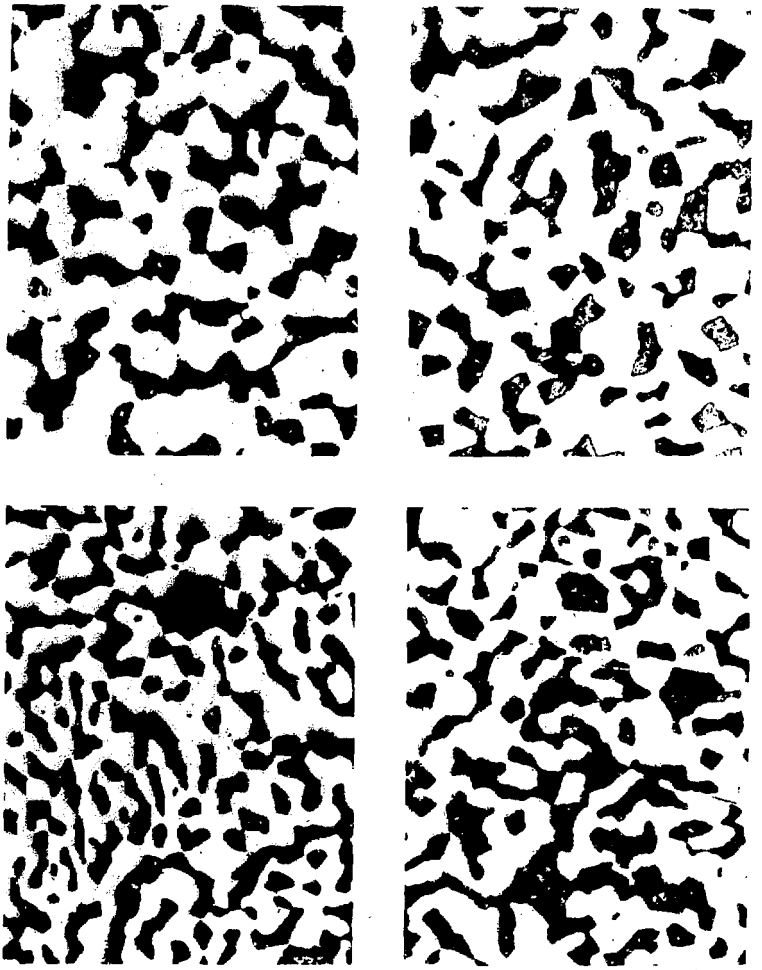

XBB782-1818

Photo 1

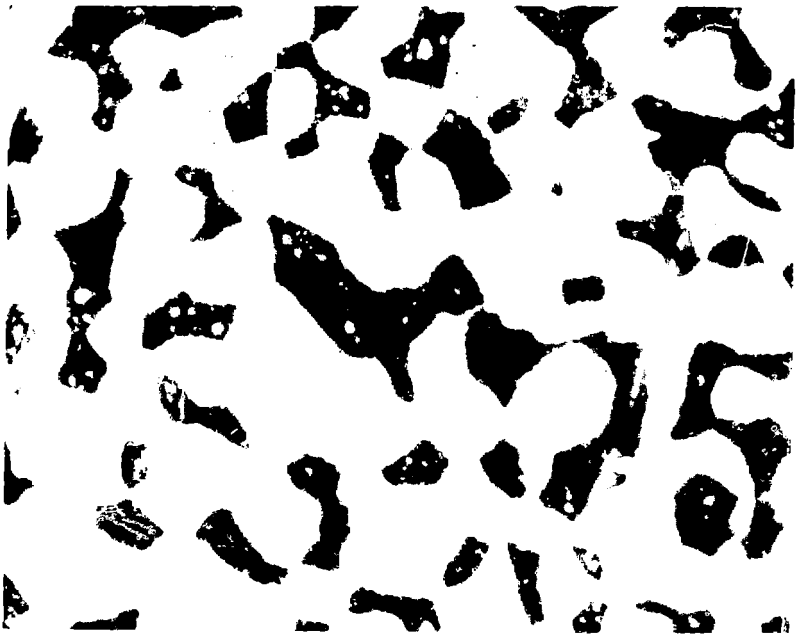

XBB782-2100

Photo 2

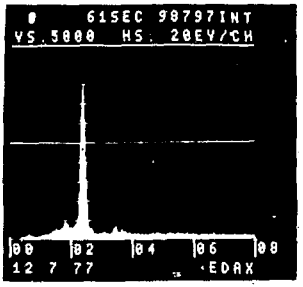

a

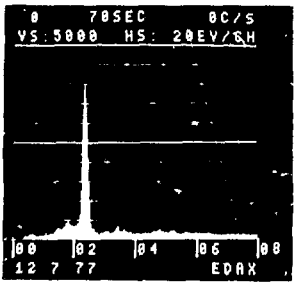

b

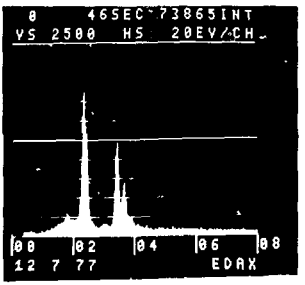

c

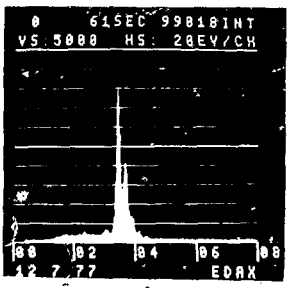

d

XBB770-13047

Photo 3

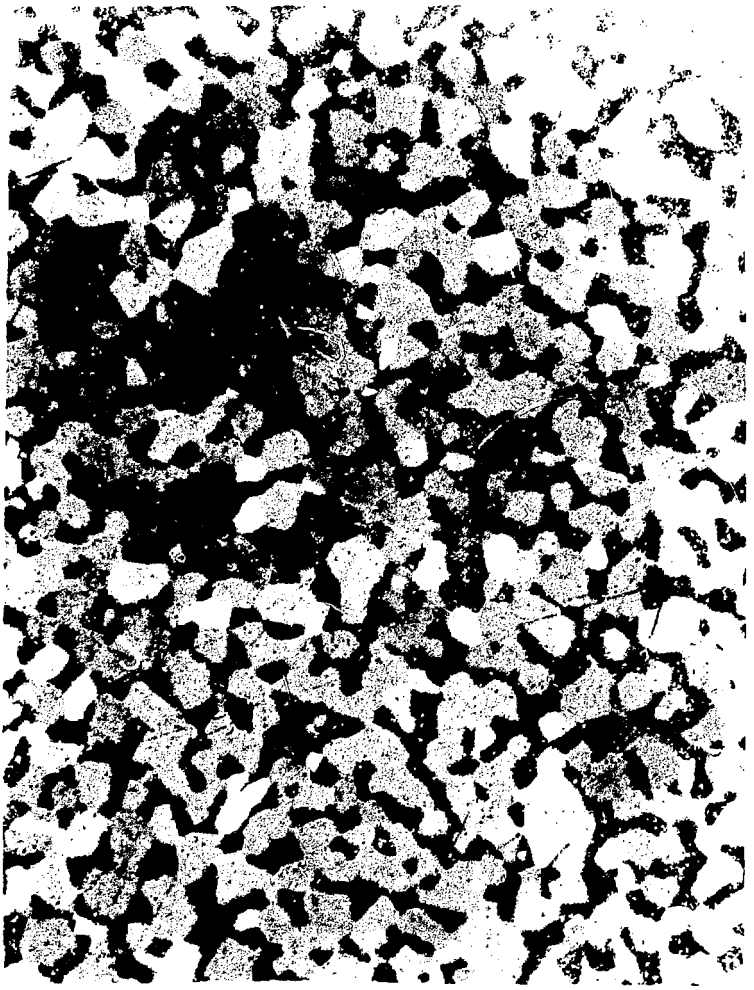

XBB782-1819

Photo 4

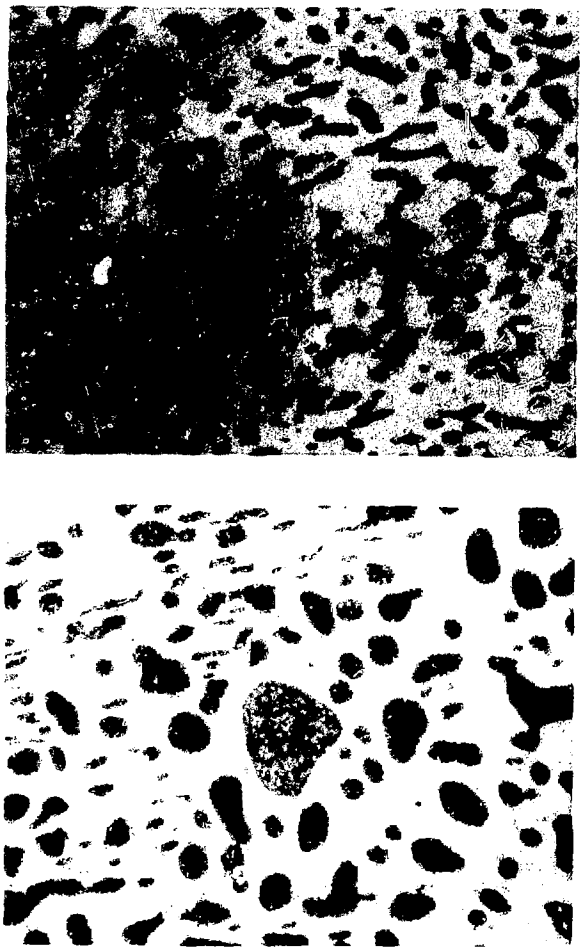

XBB782-1817

Photo 5

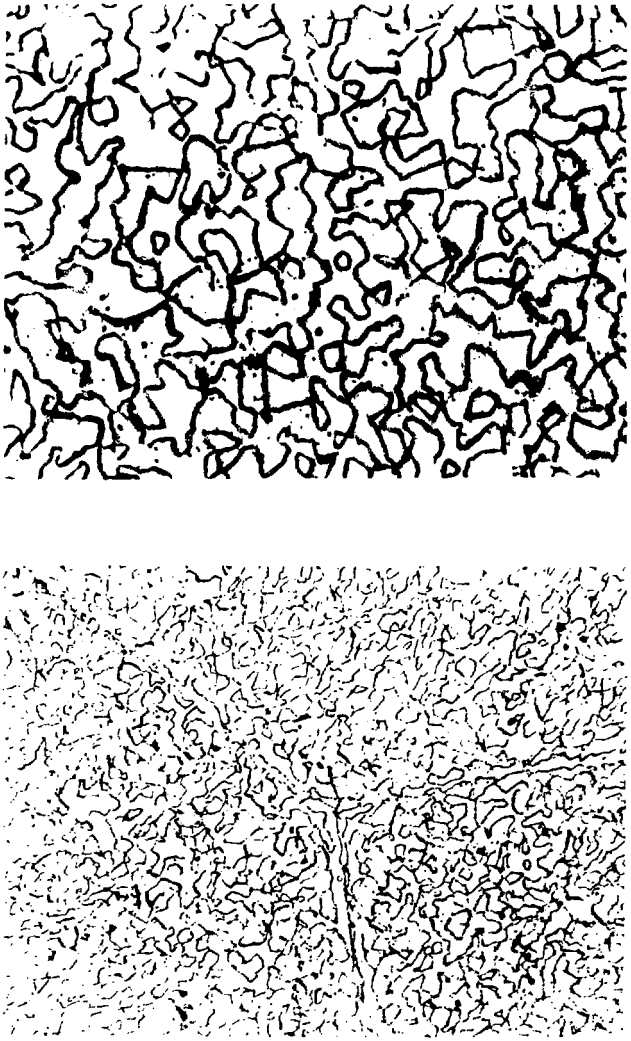

XBB770-12556

Photo 6

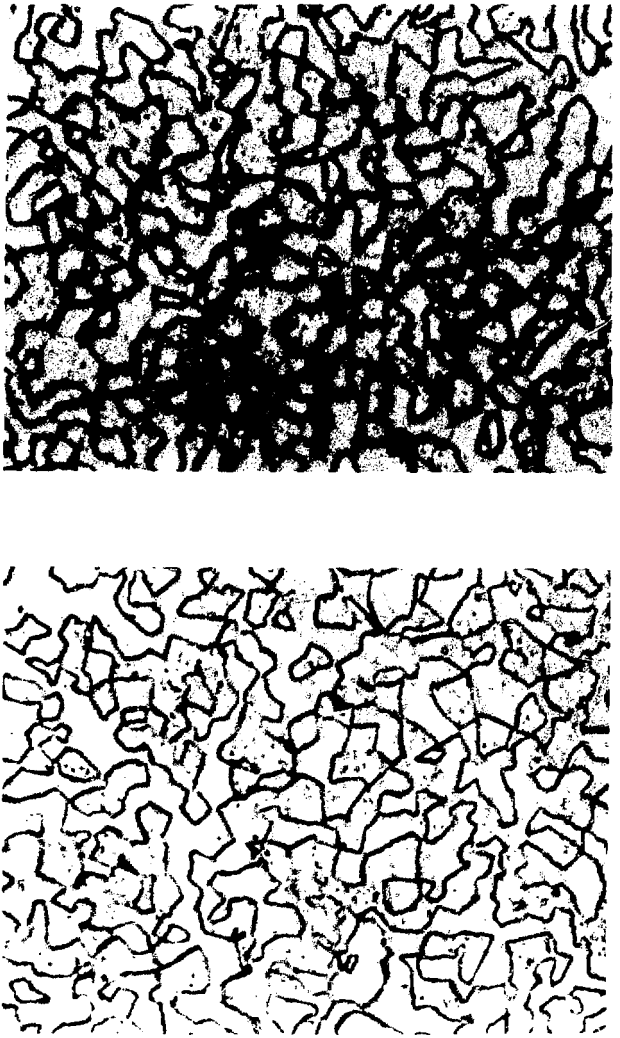

XBB770-12557

Photo 7

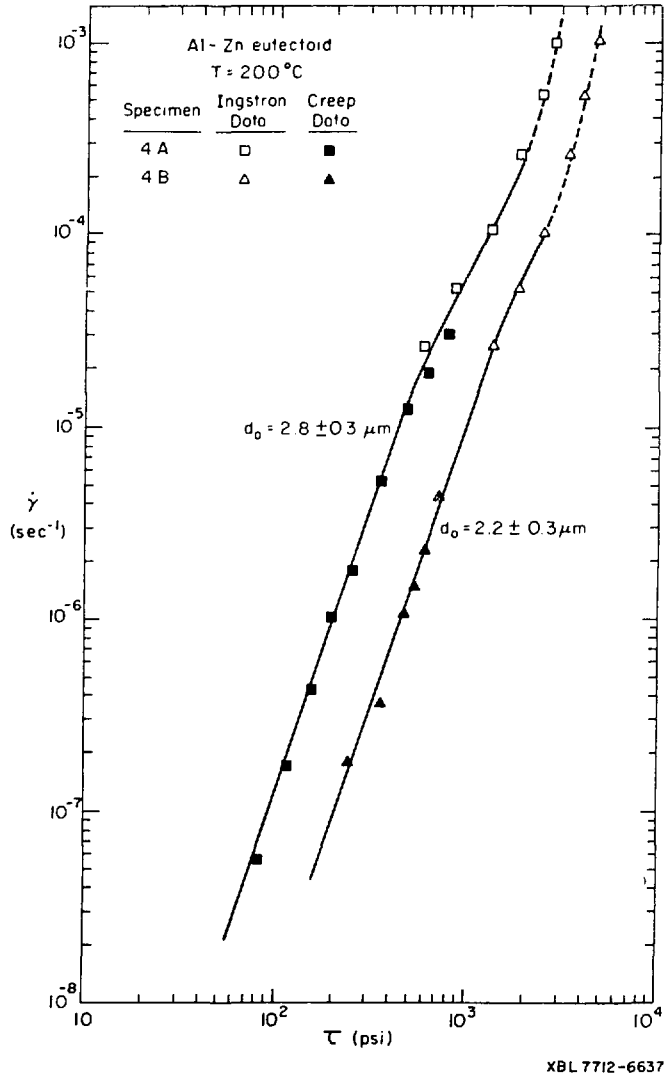
Al - Zn eutectoid
T = 200°C
Specimen
Instron Data
Creep Data
4 A
4 B
d_o = 2.8 ±0.3 μm
d_o = 2.2 ± 0.3 μm
$\dot{\gamma}$ (sec^{-1})
10^{-3}
10^{-4}
10^{-5}
10^{-6}
10^{-7}
10^{-8}
10
10^2
10^3
10^4
τ (psi)
XBL 7712-6637

Fig. 23

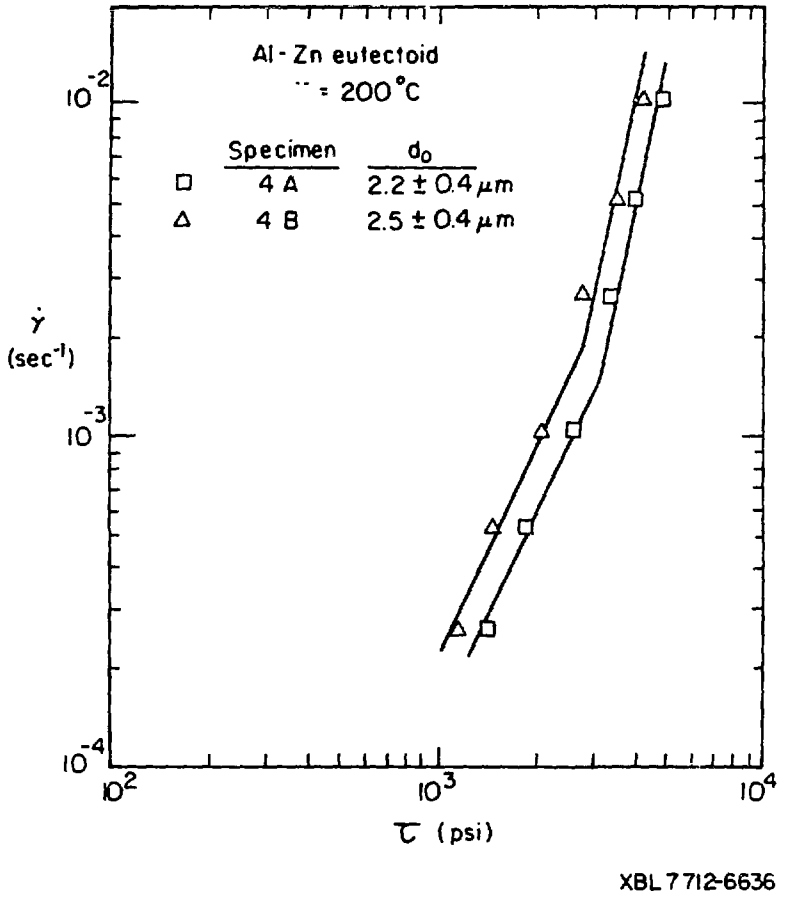
Al - Zn eutectoid
T = 200°C
Specimen
d0
4 A
2.2 ± 0.4 μm
4 B
2.5 ± 0.4 μm
γ̇
(sec⁻¹)
10⁻²
10⁻³
10⁻⁴
10²
10³
10⁴
τ (psi)
XBL 7712-6636

Fig. 24

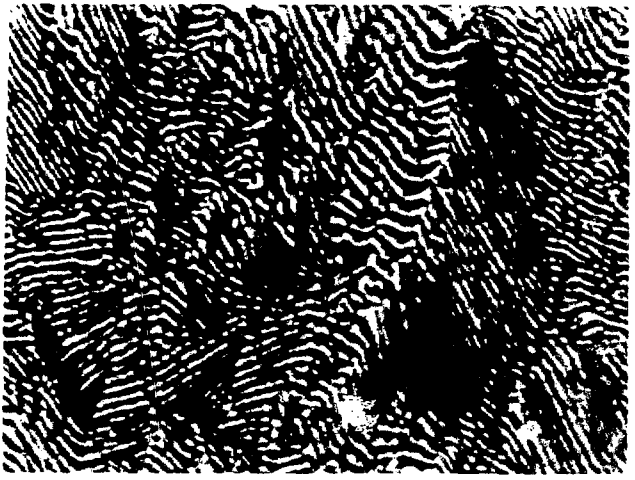

XBB770-12555

Photo 8

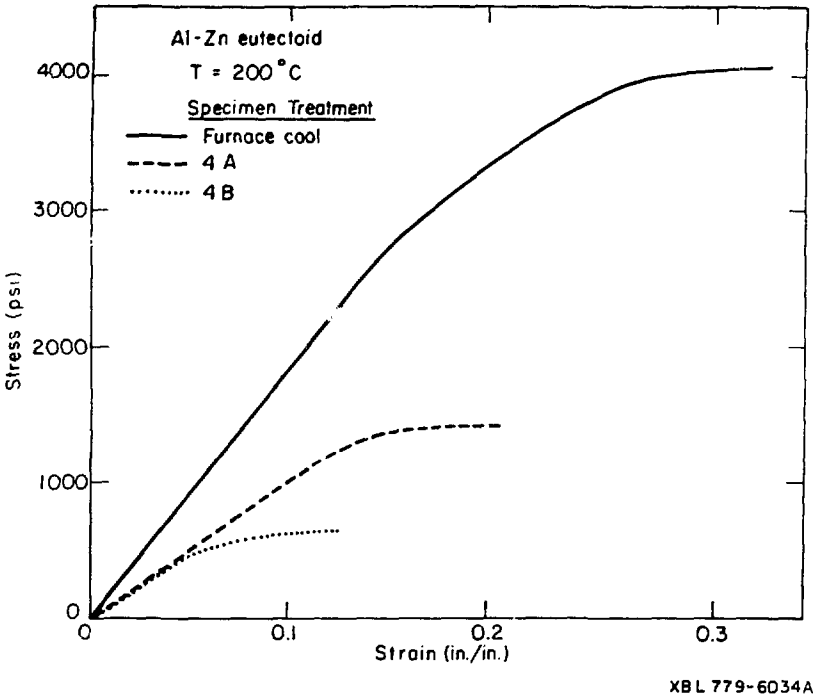

XBL 779-6034A

Fig. 25

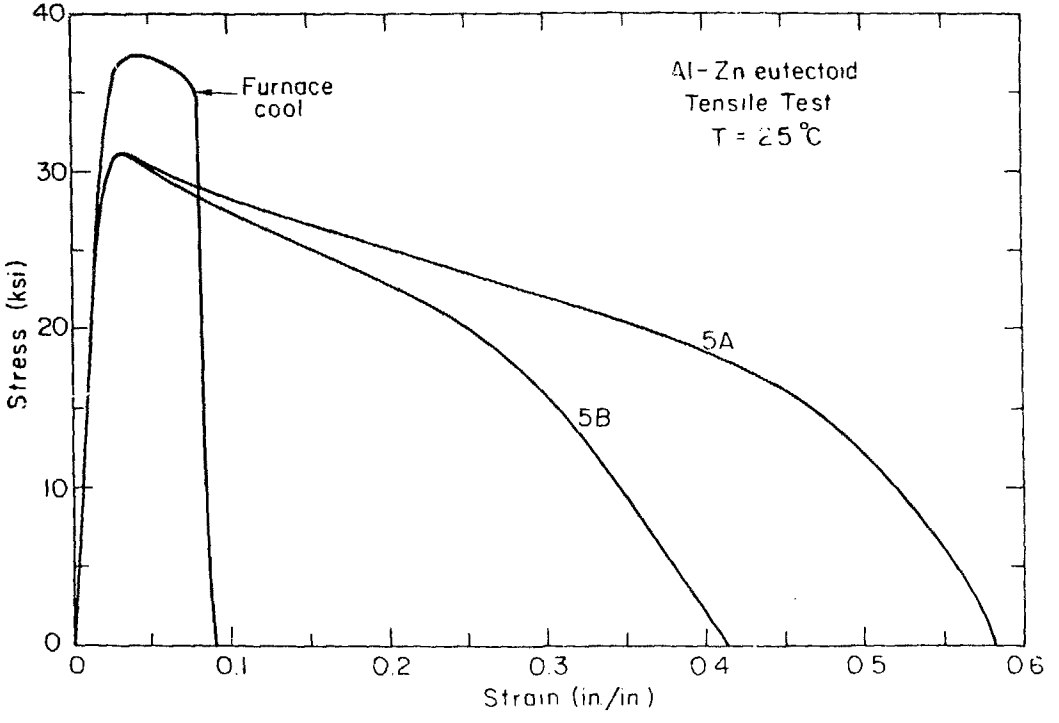

XBL7712-6646

Fig. 26

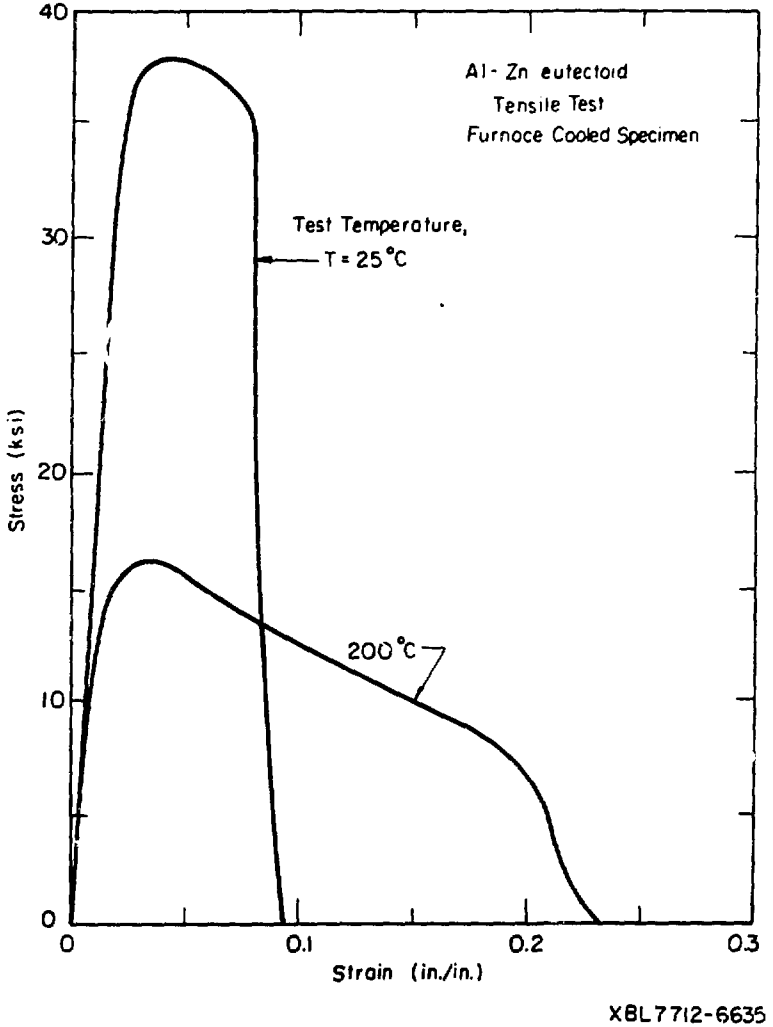
Al - Zn eutectoid
Tensile Test
Furnoce Cooled Specimen
Test Temperature,
T = 25 °C
200 °C
Stress (ksi)
Strain (in./in.)
0
10
20
30
40
0
0.1
0.2
0.3
XBL7712-6635

Fig. 27

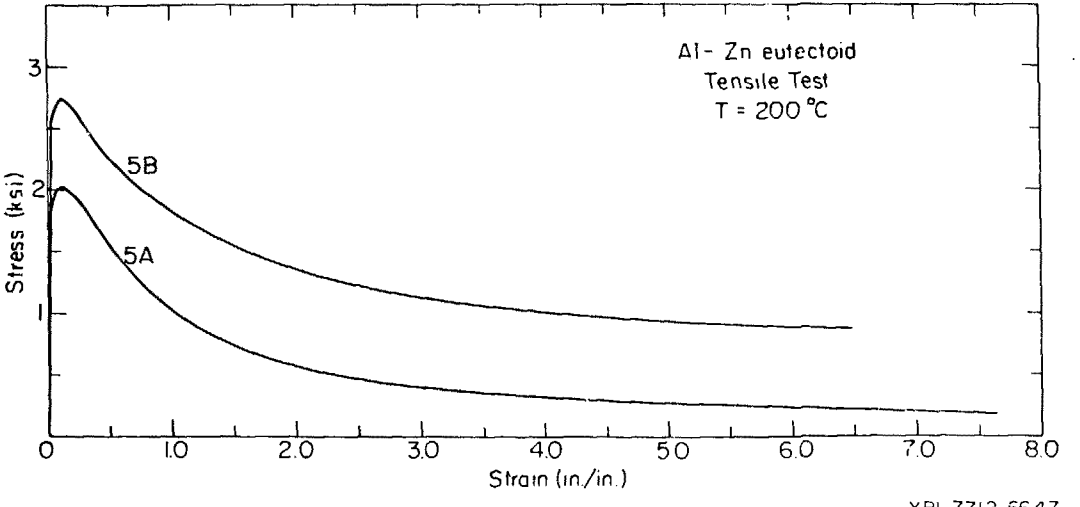
Al- Zn eutectoid
Tensile Test
T = 200 °C
5B
5A
Stress (ksi)
3
2
1
0
1.0
2.0
3.0
4.0
5.0
6.0
7.0
8.0
Strain (in./in.)
XBL 7712-6647

Fig. 28

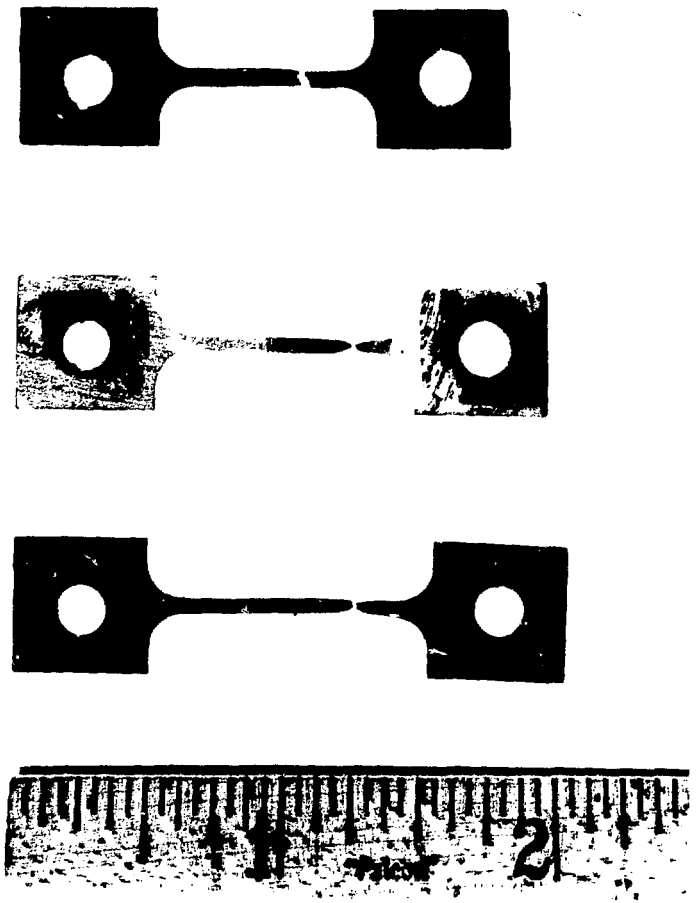

XBB770-10912

Photo 9

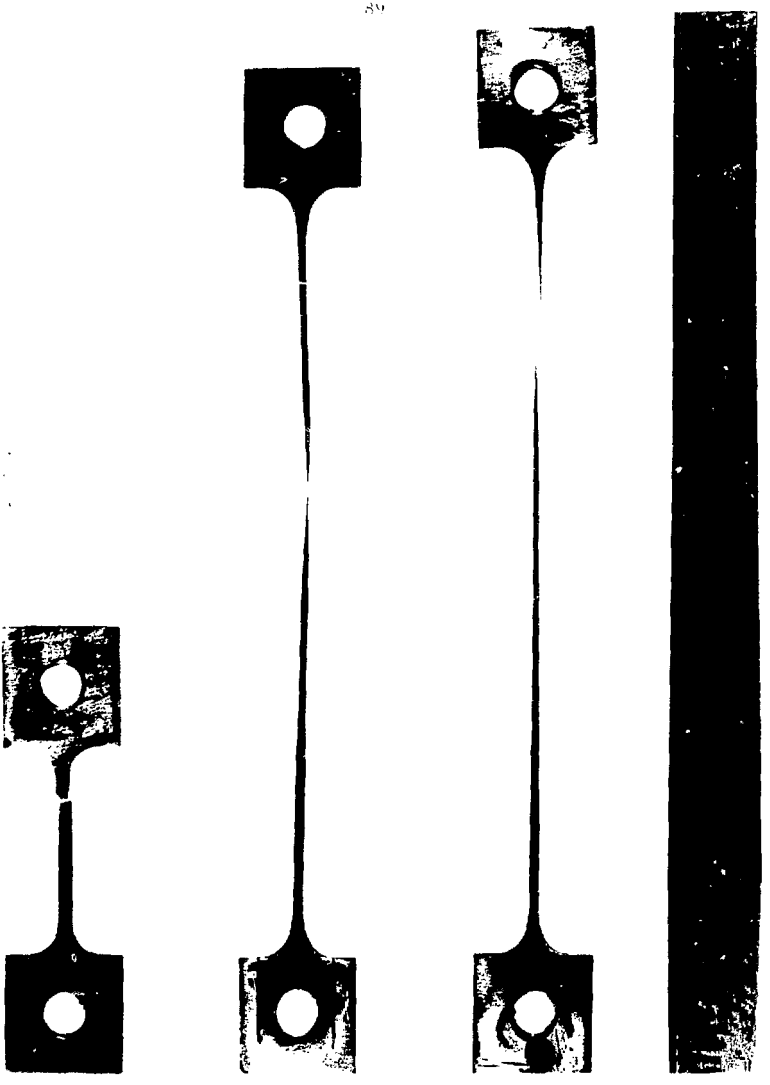

XBB770-10911

Photo 10

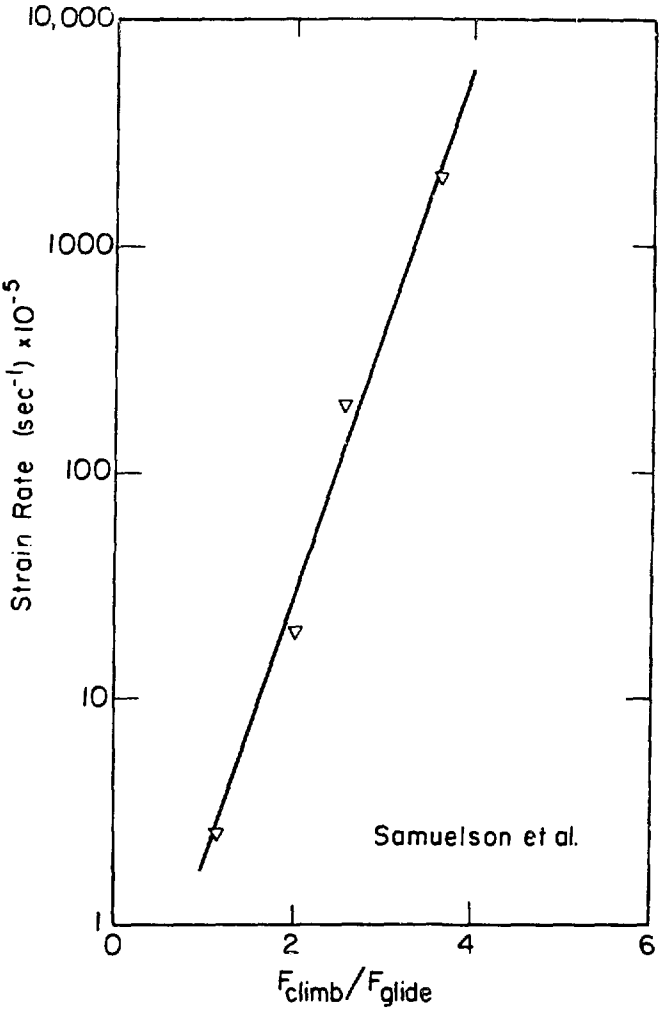
10,000
1000
100
10
1
Strain Rate (sec^{-1}) x10^{-5}
0
2
4
6
F_{climb}/F_{glide}
Samuelson et al.
XBL 7712-6631

Fig. 29